10,000 ppm Ba. Intense A.I. anomalies are also distributed. These anomalies almost overlap with the sericite-chlorite alteration zone.

Balekambang: One Au anomaly (500 ppb) and a few Pb (145 ppm), Zn (up to 1,225 ppm), Fe (up to 6.4 %) and Mn (3,900 ppm) anomalies of rock-chips were detected along S. Cipura Bangsa. A couple of A.I. anomalies was found in this area. These anomalies occur within the sericite-chlorite alteration zone.

The other locations where significant anomalies were detected in the second phase rock-chip geochemistry are as follows:

- Cisodong
- Lower Reaches of Cigoronggong
- Middle Reaches of Cigoronggong
- Upper Reaches of Cigoronggong
- Ciguranteng-Cinampak
- Pasir Gintung
- Cimomon
- Upper Reaches of Cisarua

2-4 Discussion

Several significant anomalous zones were outlined through the rock-chip geochemical survey this phase. The major anomalous zones thus defined are: Cisasah, Cikoplok-Panyairan, Cidadap, Cibuniasih, and Balekambang.

Cisasah: Several anomalies of Au (up to 1,100 ppb), Ag (up to 6.40 ppm), Cu, Pb, Zn, As, Sb, Fe (up to 20.0 %), Mn (more than 10,000 ppm) and Ba of rock-chips were found in this area. Anomalies of A.I. values are widely distributed in this area covering Cipari, Cisasah and Panyosogan. Most of these anomalies occur within the sericite-chlorite alteration zone. The A.I. values in the western part are not anomalous, although the chlorite-sericite alteration zone is exposed on the surface.

Cikoplok-Panyairan: Small Zn and Fe anomalies of rock-chips were detected along S. Cikoplok. A few anomalies of A.I. occurs at Panyairan. A pervasive sericite-chlorite alteration zone is exposed in this area covering from the lower reaches of Cikoplok up to Panyairan.

Cidadap: Several anomalies of Au, Ag, Cu (up to 4,530 ppm), Pb (807 ppm), Zn (up to 1,910 ppm), As, Sb, Fe and Mn of rock-chips were detected in this area. Anomalies of A.I. values are also concentrated in this area. These anomalies almost correspond to the sericite-chlorite alteration zone.

Cibuniasih: One Au anomaly and several anomalies of Ag (up to 64.60 ppm), Pb, Sb, Mn (more than 10,000 ppm) and Ba (more than 10,000 ppm) of rock-chips were found in this area. Intense A.I. anomalies are also distributed around Cibuniasih area. These anomalies almost overlap with the sericite-chlorite alteration zone.

Balekambang: One Au anomaly (500 ppb) and a few Pb, Zn (up to 1,225 ppm), Fe and Mn anomalies of rock-chips were detected along S. Cipura Bangsa. A couple of A.I. anomalies was found in this area. These anomalies occur roughly within the sericite-chlorite alteration zone.

The correspondence of metallic elements is very well each other. They occur concentrated at some small areas except Fe. Whereas the distribution of anomalous A.I. is rather wide. It shows that the anomalies of metallic elements tend to occur within the alteration haloes which are outlined by the distribution of anomalous A.I. values.

In the rock-chip geochemical survey, CaO, MgO, K_2O and Na_2O were analyzed along with usual geochemical elements, and the alteration index (A.I.), proposed and demonstrated in the Hokuroku Kuroko district in Japan, was introduced for the indicator of hydrothermal alteration associated with the massive sulfide mineralization. The anomalous zones defined by A.I. (A.I.≥79 %) are: Cisasah, upper reaches of Cigoronggong, Cidadap, Cibuniasih, and Balekambang. These anomalous zones occur roughly within the sericite-chlorite alteration zones outlined by the X-ray diffraction analysis. However, the correspondences between anomalous zones by X-ray and those by A.I. are not always well in details. It shows that the behaviors of these alkali metals are not numerically related to the degrees of hydrothermal alteration accompanied by the massive sulfide mineralization. Firstly, the A.I. index can not represent the alterations accompanied by strong silicification, such as footwall silicified zone with sericite alteration, and gypsum zone with silicification and sericitization. Secondly, it is only applicable within the sericite-chlorite alteration zone. It is not useful in the entire regional alteration zoning -- sericite-chlorite zone through montmorillonite-kaolin zone to zeolite zone.

Chapter 3 Gravity Survey

Gravity survey was carried out in the Cisasah-Cidadap-Cibuniasih area for the purpose of clarifying the basement structure and the geological setting of the massive sulfide deposit.

3-1 Survey Method

As shown in the flow chart (Fig. 2-7), the process of gravity survey is largely grouped into "field survey", "data processing" and "analysis".

3-1-1 Field Survey

(1) Gravity measurement

a. Stations

Gravity survey area is shown in Fig. 1-2. Gravity measurement was carried out at 316 stations in an area of about 340 km^2 . The location of the stations is shown in Fig. 2-8 . The station interval was about 500m to 1 km along the traverse.

b. Instrumentation

Two sets of LaCoste G gravimeters were used for the field measurement. This gravimeters were selected considering its extremely good transportability, ease of operation and accuracy of measurement. The specifications of the LaCoste gravimeters used are as follows.

Gravimeter No.	G-178	G-365
Year of manufacture	Feb.1968	Mar.1974
Operating range	0~7,344.88 mgal	0~7,447.81mgal
Accuracy	0.02 mgal	
Size	14 x 15 x 20 cm	
Weight	8.6 kg	
Power source	12 V battery	
Manufacturer	LaCoste & Romberg(USA)	

The milligal constant(K) and scale constant(κ) for the range used in this survey are as follows.

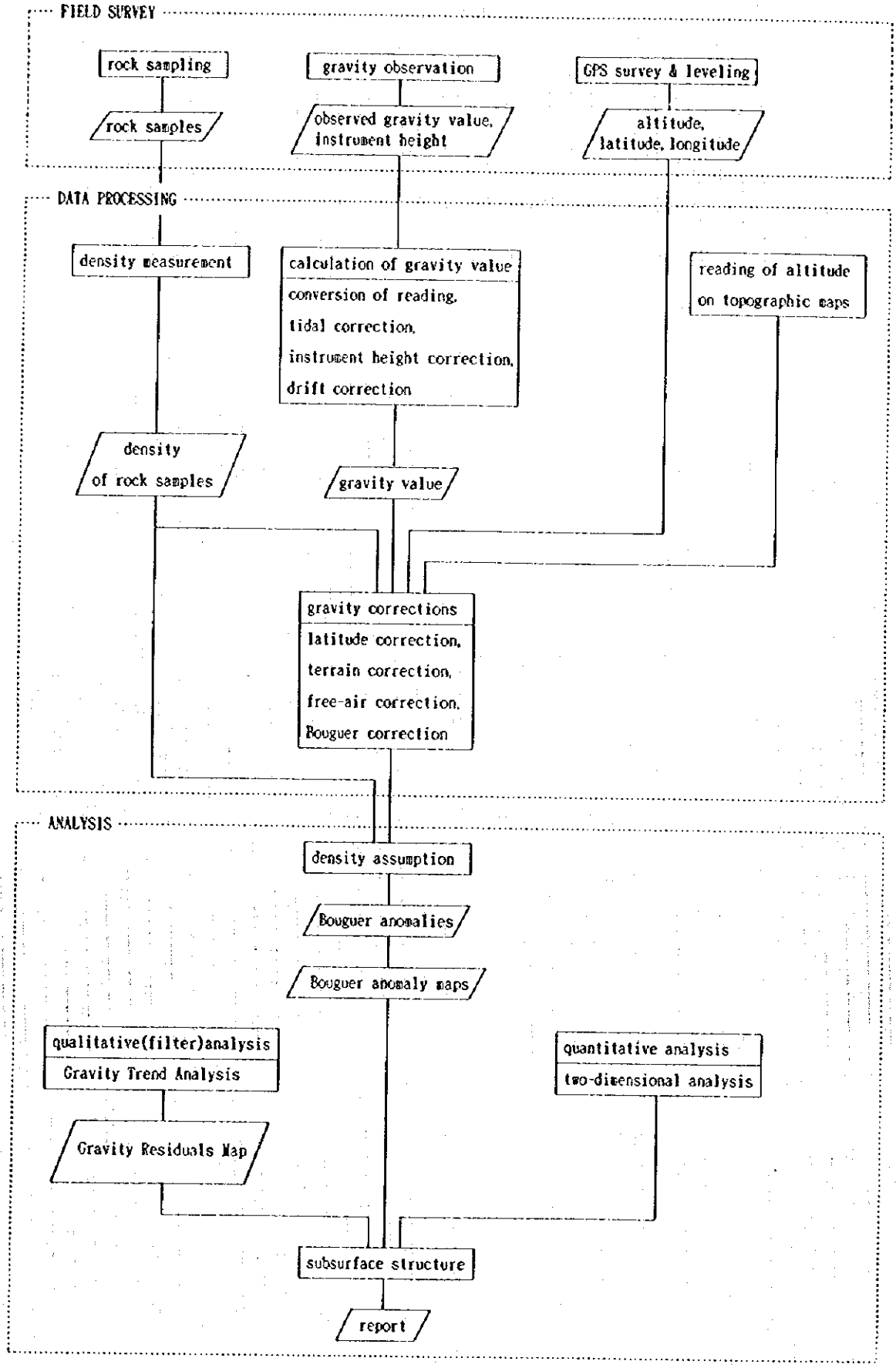

Fig. 2-7 Gravity Survey Procedure

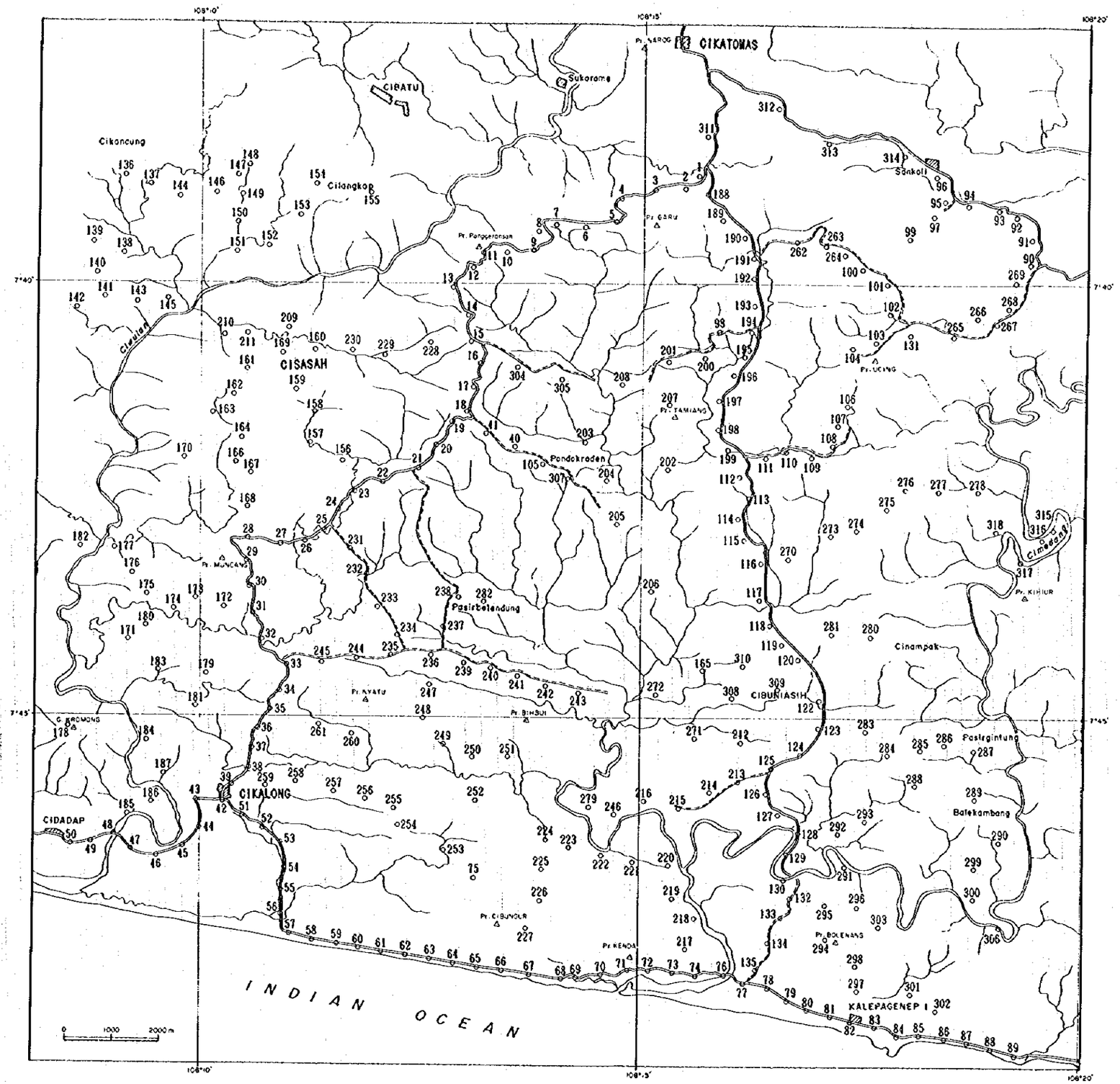

Fig. 2-8 Location Map of Gravity Stations

Gravitymeter No.	Counter reading	Milligal constant	Scale constant
G - 178	1500	1569.99	1.04725
	1600	1674.71	1.04736
	1700	1779.45	1.04748
	1800	1884.20	1.04760
G - 365	1600	1702.31	1.06358
	1700	1808.67	1.06359
	1800	1915.03	1.06361
	1900	2021.39	1.06363

c. Gravity reference station and base station

The reference station for this survey is called DG.0 at the G.S.I.headquarters in Bundung. The gravity value of this reference station is as follows (Adkins,J.et al.,1978).

St.No.	Elevation	Latitude	Longitude	Gravity value
DG.0	718.0 m	06°53.90'S	107°37.90'E	977,976.38 mgal

The gravity base station was established at the following location for starting and terminate point for each survey route.

St.No.	Elevation	Gravity value	Location
1000	252.6m	978,192.43 mgal	Front of the house at Jl.Raya No.135,Cikatomas

The gravity value of this base station was determined by base tie from the gravity reference station DG.0. The detailed map of the location and photograph of these two stations are shown in App. 3.

(2) Leveling and positioning

The leveling and positioning of the stations were mainly done by GPS(Global Positioning System) static survey which uses the signals from satellites. This was augmented by conventional leveling .

a. Instrumentation

Three sets of 4000ST GPS surveyors (Trimble Navigation Ltd.) and two sets of Wild T-0 automatic level .

b. GPS survey

Relative positioning of the GPS was employed. In this method, the satellite signals are receiving simultaneously at the base and the measurement station. Then the position of the station is calculated relative to that of the base. By this method, vertical accuracy of

several centimeters can be obtained by one hour observation and of less than one meter by 5 to 20 minutes observation.

The GPS base station was established at the front yard of Kantor Camat Cikatomas. The elevation of the GPS base station was determined by one hour relative positioning observation with the Triangulation station No. 250 at Pasir Nagrog of elevation 359.0m.

For ordinary measurements, 6 to 30 minutes observation was necessary depending on the number and location of available satellites.

From GPS survey , latitudes and longitudes based on WGS-84 (World Geodetic System) ellipsoid are obtained. These were converted to coordinates used in Jawa by comparing at several stations where the coordinates are known.

Of the 316 stations established, 256 were positioned by GPS method.

c. Leveling

The 60 stations were positioned by conventional leveling . Almost of them were along the coast where the environment was suitable for conventional leveling because of small difference of elevation along the traverse.

(3) Rock sampling

Rock samples for density measurements were collected throughout from the survey area with due consideration of the stratigraphy, lithology and other relevant factors. The number of collected samples amounted to 100 and the localities are shown in Fig. 2-9. Twenty-two samples were also collected from the drilling core of MIT-5 .

3-1-2 Data Processing

Data processing for gravity survey largely consists of the following two parts.

- Calculation of gravity values from the dial readings (gravity calculation).
- Calculation of Bouguer anomalies (gravity reduction).

(1) Calculation of gravity values

In order to calculate the gravity values from the dial readings, following processes are carried out.

-milligal conversion
-tidal correction
-instrument height correction
-drift correction

These are processed on the basis of the "original data file" prepared for each station. This file contains; station number, date and time of measurement, gravimeter dial reading, instrument height, latitude, longitude, elevation, terrain correction of "neighbor", code number

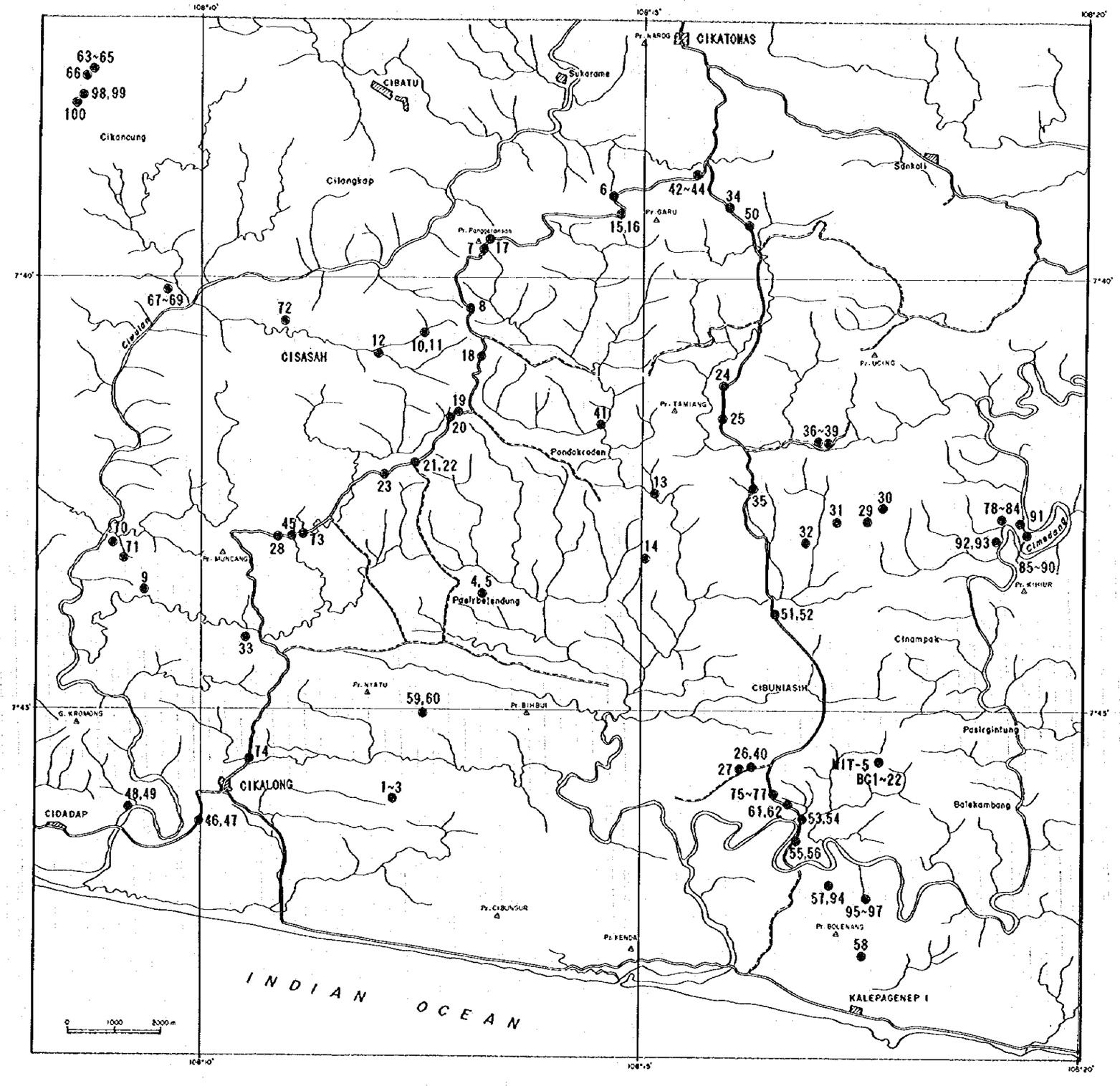

Fig. 2-9 Location Map of Density Samples

of gravimeter, leveling method, terrain correction of "close" by the format of 80 figures. Detail method of calculations is shown in App.4.

(2) Gravity reduction

The process of calculating the Bouguer anomaly values is called the gravity reduction and it consists of following calculations.

-latitude correction
-terrain correction
-atmospheric correction
-free air correction
-Bouguer correction

Detail method of calculations is also shown in App.4.

(3) List of gravity values

Tables of relevant data regarding this gravity survey are attached in the Appendices 5, 6 and 7. These data include; location (coordinates and elevation) of stations, gravity values, various correction values, normal gravity values and Bouguer anomalies, and Bouguer anomalies for eight different assumed density values.

(4) Preparation of gravity maps

The Bouguer anomaly value of each station was converted to grid point value on rectangular coordinates. This was done in order to draft Bouguer anomaly map using a plotter and to obtain gravity values for filter analysis.

La Porte(1962) method was used for calculating the values for the grid points because the reproducibility of the Bouguer anomaly for each station is very good by this method. The grid interval of 1 km was used and the grid point values were calculated only when more than six stations were included within a range of 10 km radius with over 240 degree angle with the center at the grid point. Four types of Bouguer anomaly maps were prepared with correction densities of 2.00,2.10, 2.20 and 2.30 g/cm^3.

3-1-3 Analytical Method

(1) Density estimation

a. Density measurement of rock samples

The density of the collected samples was measured by the following formula.

$$\text{Natural dry density} = \frac{W_1}{W_2 - W_3} \qquad (3\text{-}1)$$

$$\text{Wet density} = \frac{W_2}{W_2 - W_3} \qquad (3\text{-}2)$$

W_1 : Weight in air of samples left in a room (normal temperature) for several days (naturally dried)
W_2 : Weight in air of samples immersed in water for 24h under natural atmospheric pressure and the surface was wiped with cloth
W_3 : Weight in water after immersion for 24h under natural atmospheric pressure

b. Gravity profile with density

A reasonably satisfactory estimate of the near-surface density is obtained from a representative gravity profile over the survey area. Calculate the gravity profiles for corrections of assuming several different densities along relatively rugged topography. The smoothest of these profiles, that is, the one which reflects the topography least, is the one with the correct density.

(2) Gravity analysis

a. Gravity trend analysis

This method is used for isolation of local anomalies from regional anomaly field due to crustal structure.

Regional anomaly field is obtained by polynomial fitting. The observed data are used to compute, by least squares, the mathematical surface giving the closest fit to the gravity field. In practice the surface is expressed mathematically as a two-dimensional polynomial of low order.

A 1st-order polynomial is expressed as

$$G_1(x,y) = A_0 + A_1 x + A_2 y \qquad (3\text{-}3)$$

A 2nd-order as

$$G_2(x,y) = A_0 + A_1 x + A_2 y + A_3 x^2 + A_4 xy + A_5 y^2 \qquad (3\text{-}4)$$

A 3rd-order as

$$G_3(x,y) = A_0 + A_1 x + A_2 y + A_3 x^2 + A_4 xy + A_5 y^2 + \cdots\cdots + A_8 xy^2 + A_9 y^3 \qquad (3\text{-}5)$$

A n-order polynomial is expressed as

$$G_n(x,y) = A_0 + A_1 x + A_2 y + A_3 x^2 + A_4 xy + A_5 y^2 + \cdots\cdots + A_{m-1} xy^{n-1} + Am\, y^n \qquad (3\text{-}6)$$

$$m = n(n+3)/2$$

The coefficients A_0, A_1, ..., etc. are determined by a least-square adjustment. Then the gravity residuals (local anomalies) are obtained by subtracting the polynomial values from the observed gravity values.

b. Profile analysis

The profile analysis is a quantitative analysis aimed at constructing a two dimensional model of the subsurface structure which would result in gravity anomalies approximating most closely those measured in the area. The gravity anomalies of the model are calculated by the following Talwani et al.(1959) equation.

$$g = 2\,G\,\Delta\rho\,\sum Z_i \tag{3-16}$$

$$Z_i = A_i \sin\phi_i - \cos\phi_i \{\theta_i - \theta_{i+1} + \tan\phi_i \log \frac{\cos\theta_i\,(\tan\theta_i - \tan\phi_i)}{\cos\theta_{i+1}(\tan\theta_{i+1} - \tan\phi_i)}\} \tag{3-17}$$

g : Gravity anomaly value
G : Gravitation constant
Δρ : Density constant ($\rho_2 - \rho_1$)

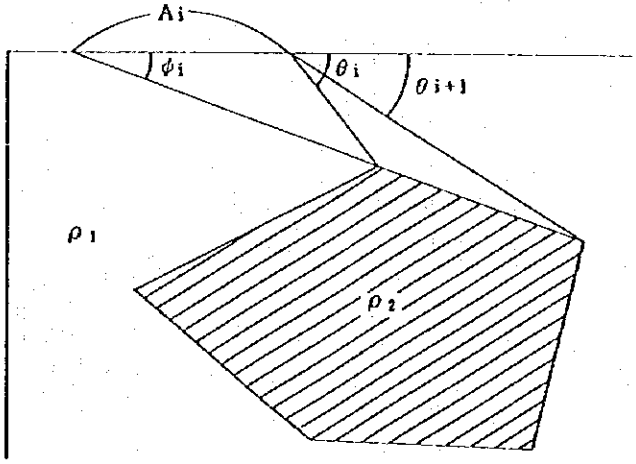

Schematic analysis of two-dimensional density structure by Talwani's method

When the subsurface density structure can be approximated by two-layered model, unique solution can be obtained by; designating a density contrast and a control depth, and then gradually altering the shape of the density boundary thus approximating the calculated values closer to the measured values. This method is very effective when the actual subsurface density structure can be approximated by two-layered structure, and good solutions can be obtained in short time. During this survey, two-layered model analysis was used for the first-order gravity residuals.

3 - 2 Survey Results

3-2-1 Density Determination

(1) Density measurements

The results of the density measurements of the 100 rock samples and 22 drilling core are shown in App.8. And the average wet density of each formation and rock is shown in Table 2-7. The average wet density of the 100 rock samples is 2.18 g/cm^3.

(2) Density profile

Fig 2-10 shows gravity profiles for assuming various densities with topography. The criterion for the actual near-surface density is that which gives the smoothest reduced curve for the Bouguer anomaly and shows least visible (direct or inverse)correlation with the topography.

This profile indicates that correct density appears to be ρ = 2.40 g/cm^3 in the south of the area , and ρ = 2.00 g/cm^3 in the north of the area. Therefor ρ = 2.20 g/cm^3 is a good assumption for whole area.

3-2-2 Bouguer Anomaly Map

Four types of Bouguer anomaly maps were prepared, namely ρ =2.00, 2.10, 2.20 and 2.30 g/cm^3. Comparing the four types of Bouguer maps, the distribution of the gravity anomalies is similar for all of them. Thus, the subsequent interpreted results probably would not differ very much among the four maps. From the density measurements and density profile, Bouguer anomaly map with ρ =2.20 g/cm^3 was selected (Fig. 2-11).

According to the Bouguer anomaly map of the survey area, Bouguer anomaly is lower in the north and higher in the south in general. The highest Bouguer anomaly (167 mgal) occurs near Cidadap in the southwestern part of the area. The lowest anomaly (118 mgal) occurs at the southeast of Sankali in the northeast part of the area. Distance of these two points is about 24 km, therefor Bouguer anomaly increase from NNE to SSW with a steep gradient of about 2mgal / km. This prominent regional anomaly field is no relation of geological setting shown in Fig. 2-1 and is due to broad crustal structures.

As for the local anomaly, remarkable gravity lows is extending over Pasir Nyatu and Pasir Bihbui. Gravity highs occur near Pasir Garu, near Pasir Belendung, near Cidadap and in the south of Balekambang. Gravity lows occur in the southeast of Sakali, Cibatu, Pasir

Table 2-7 Average Rock Density (Wet)

Age	Formation		Rock name	Number	Average density(g/cm³)	
Pliocene	Bentang		Limestone	8	2.17	1.98
Late Miocene	Bentang		Calcareous Sandstone	25	1.91	
Late Miocene	Kalipucang		Limestone	21	2.34	2.31
Middle ~Early Miocene	Kalipucang		Calcareous Sandstone(surface)	2	2.00	
			(drilling core)	2	2.33	
Oligocene	Jampang	Upper	Tuff (surface)	21	1.88	1.91
			(drilling core)	20	1.94	
	Jampang	Lower	Andesitic Volcanic Breccia	2	2.29	2.67
			Andesitic Volcanic Breccia (Andesite Fragment)	7	2.68	
			Andesite	7	2.78	
	Intrusives		Andesite	7	2.64	

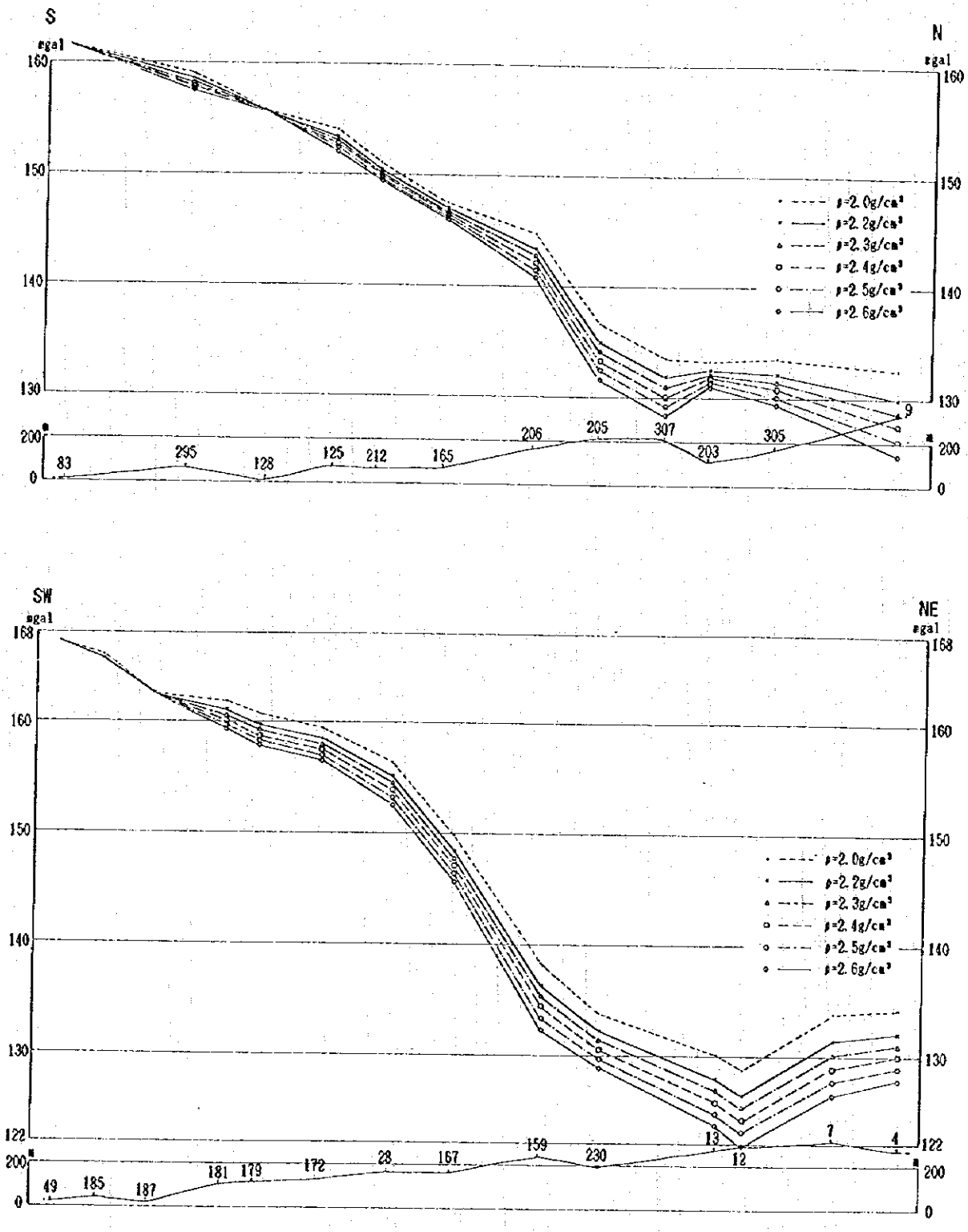

Fig. 2-10 Gravity Profile for Various Densities with Topography

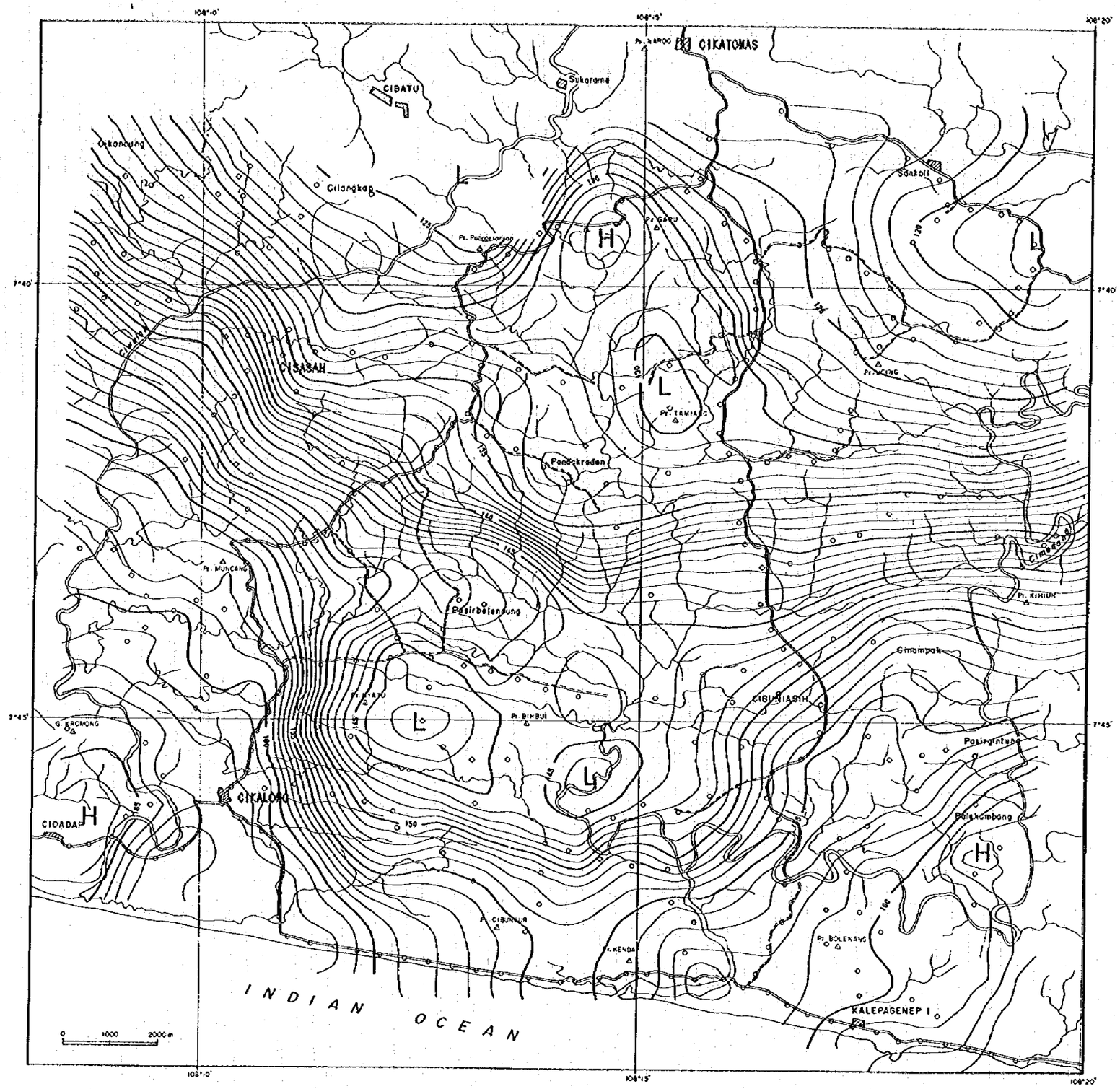

Fig. 2-11 Bouguer Anomaly Map (ρ=2.2 g/cm³)

Tamian, Pondokraden and south of Cikalong. And there are some irregularity of the contours like near Cisasah.

But for understanding the scale and location of these local anomalies, regional anomaly field must be removed.

3-2-3 Gravity Trend Analysis

(1) Gravity trend

Fig. 2-12 shows the first-, the second- and the third-order gravity trend map. These indicate regional anomaly field due to broad crustal structure. Comparing these three maps, general figure of anomaly that is lower in the north and higher in the south(ocean side) is the similar. In the higher order map, the contours, however, become denser and anomaly values become higher in the eastern and the western fringe of the survey area. Gradient is 2.3 mgal/km in the first-order gravity trend.

(2) Gravity residuals

Fig. 2-13 shows the first-, the second- and the third-order gravity residuals map. These are obtained by subtracting the gravity trend (Fig. 2-12) from the Bouguer anomaly values (Fig. 2-11). These indicate local anomalies related relatively shallow structure. Comparing these three maps, gravity lows occur about the same location. Though gravity highs occur closer to the central part of the survey area in the higher-order because of lower anomaly values in the eastern and the western fringe area. Gravity highs of the second- and third-order do not coincide with the distribution of the Lower Member of the Jampang Formation outcrop considered as basement. Therefore for the succeeding analysis, the first-order gravity residuals are selected as considering smallest distortion in the fringe area.

(3) Local anomalies on the first-order gravity residuals map

The first-order gravity residuals map is shown in Fig. 2-14. Local anomalies recognized on this map is as follows.

Gravity highs are :

- H_1 middle reaches of Ciwulan (named Middle Ciwulan uplift)
- H_2 near Pasir Garu (named Pasir Garu uplift)
- H_3 near Pasir Gintung (named Pasir Gintung uplift)

Gravity lows are :

- L_1 from Pasir Nyalu to the lower reaches of Cimedang (named Cikalong basin)
- L_2 near Pasir Panggeransan
- L_3 near Pondokraden
- L_4 east of Pasir Ucing (L_2, L_3 and L_4 are named Cibongas basin)

Steep gravity gradients reliable with sufficient stations are :

First-order

Second-order

Third-order

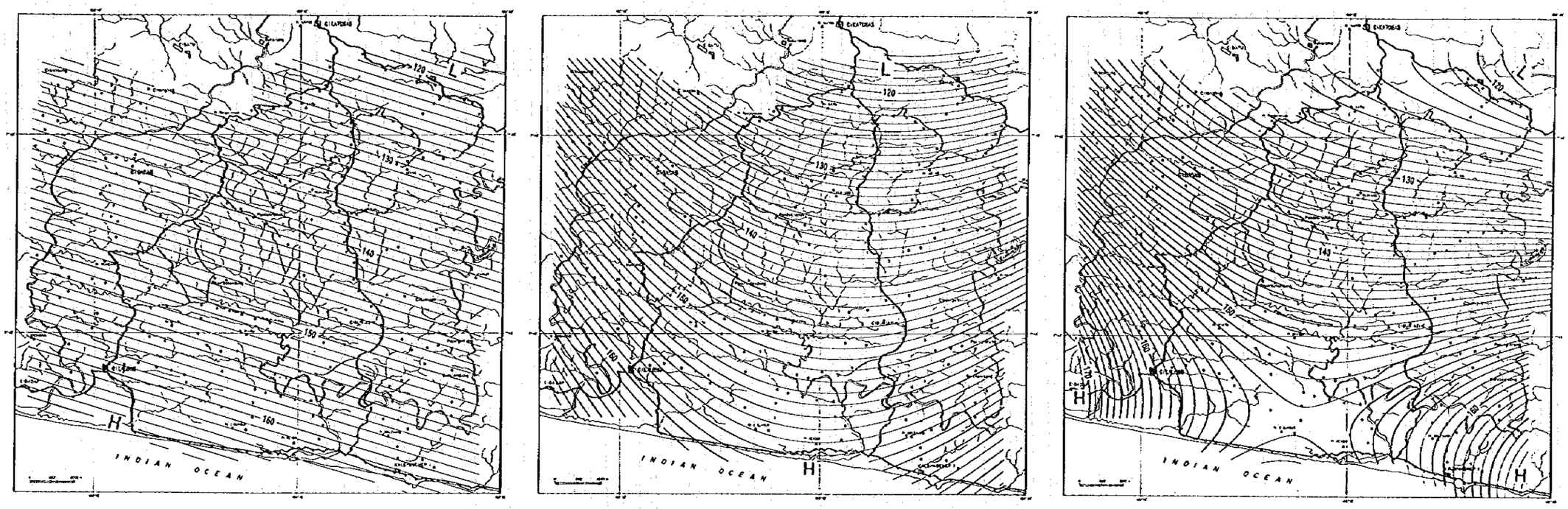

Fig. 2-12 Gravity Trend Maps

First-order

Second-order

Third-order

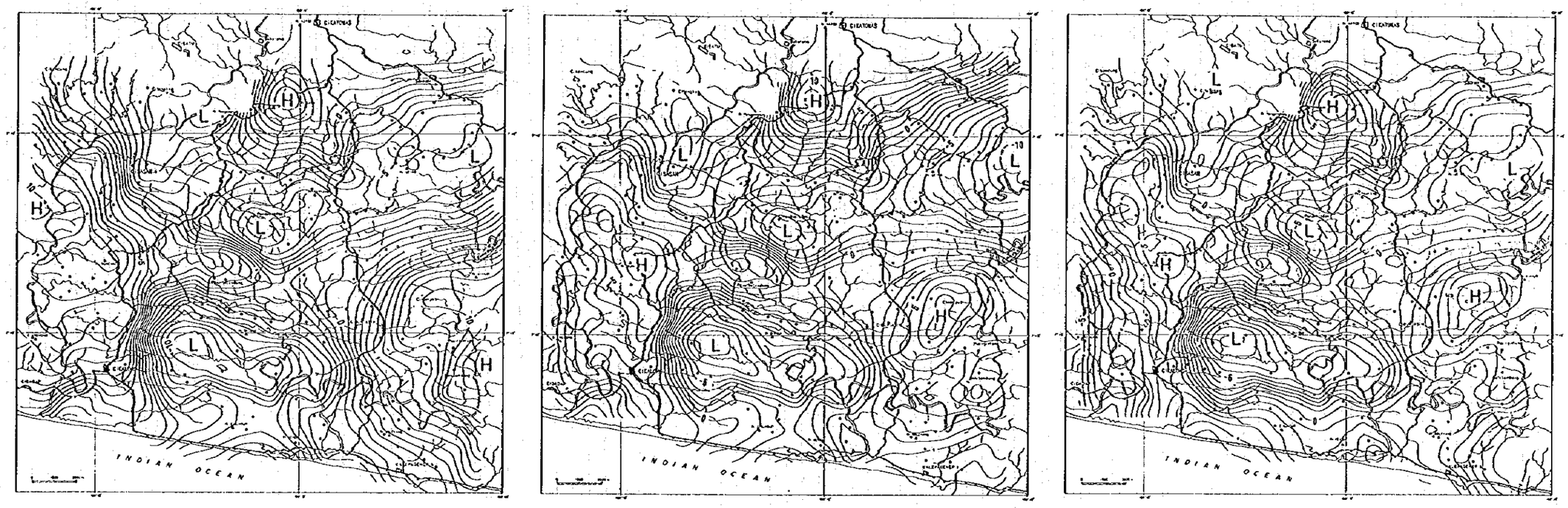

Fig. 2-13 Gravity Residuals Maps

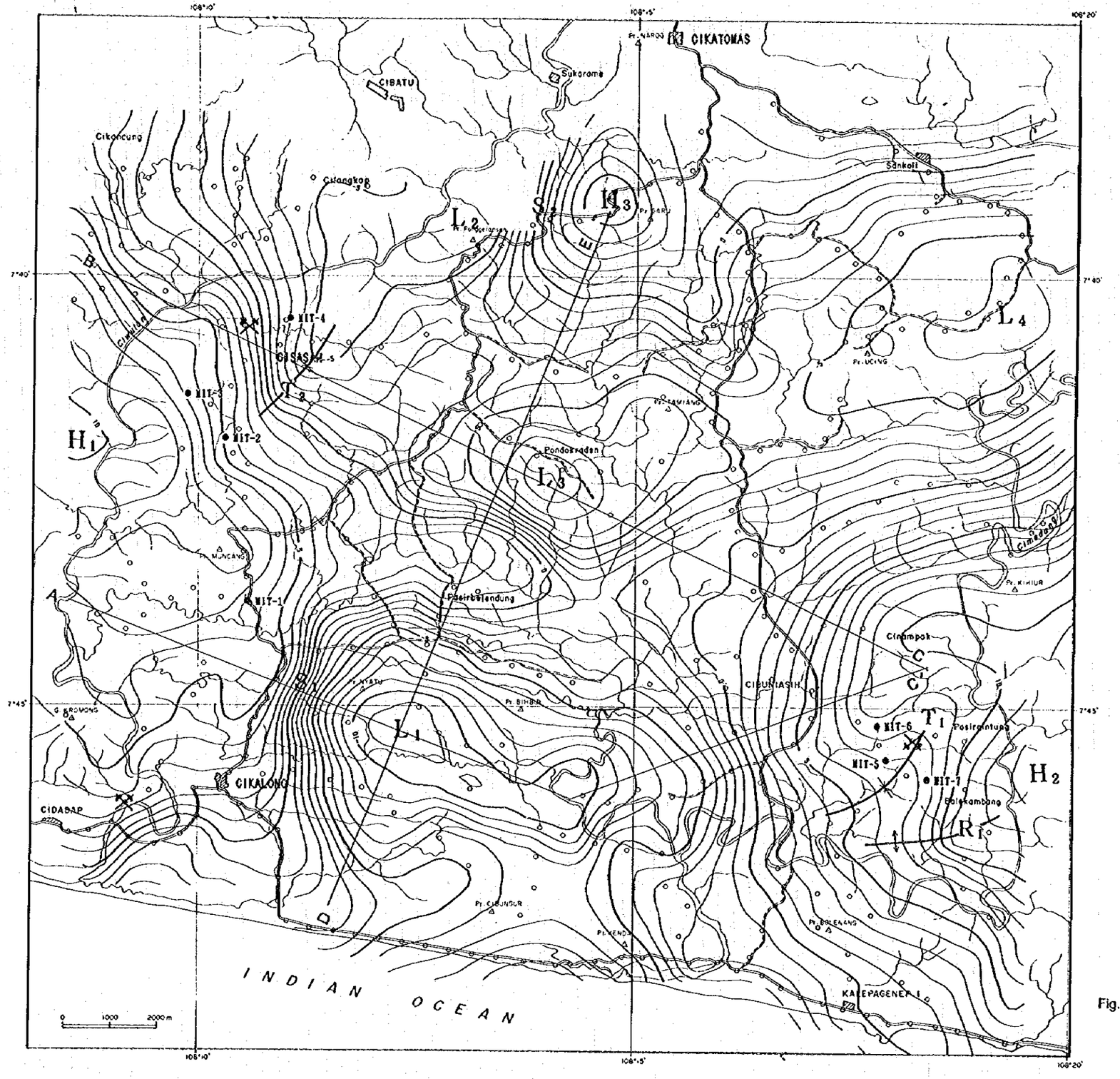

Fig. 2-14 First-Order Gravity Residuals Map

S_1 west and northwestern side of gravity low L_1

S_2 western side of gravity high H_3

The gravity highs H_1, H_2 and H_3 coincide well with the distribution of the Lower Member of Jampang Formation outcrop. Therefore they are considered to be the uplifts of the basement.

L_1 is the most remarkable gravity low and shows a basin-like structure (Cikalong basin). This basin is about 10 km from east to west and 6 km from north to south. To its west and northwest, the gravity gradient is steep westward to the Cikalong-Cikatomas road and northward to Pasir Belendung (S_1). The eastern slope, in contrast, is relatively gentle and goes up to the gravity high H_2 . The gravity low L_3 continues eastward to L_4 and northwestward to L_2. This gravity low zone is named the Cibongas basin and is divided from L_1 (Cikalong basin) by E-W gravity high from H_1 to H_2. The shapes of the northern side of H_3 and L_2 are not reliable because these anomalies occur at the northern margin of the survey area where sufficient amount of stations don't exist.

Steep gravity gradients S_1 and S_2 suggest steep change of the basement depth. S_1 could be interpreted as N-S and E-W faults and S_2 as N-S faults. Another less steep gradients is found at the east of the Cisasah gypsum mine. It may be interpreted as the northbound extension of S_1.

In Cibuniasih area, the gravity contours make a trough T_1 and a ridge R_1. These coincide very well with the syncline and the anticline by the aerial photo analysis. Another trough T_2 is found at near Cisasah. The relation between these troughs and mineral deposits are interesting.

The known gypsum mines, at Cisasah and Cidadap, and barite bed at Cibuniasih lie on the flank of the gravity structure between the gravity high and gravity low.

3-2-4 Two-Dimensional Profile Analysis

The two dimensional analysis was carried out for three profiles A-C', B-C, and D-E shown in Fig. 2-14. A-C' and B-C profiles pass through almost the same area as the geological cross sections. Objective of this analysis is the quantitative analysis of the structure of the upper surface of the Lower Member of the Jampang Formation as the basement surface.

Area of the Lower Member of the Jampang Formation outcrops show marked high gravity anomaly. Its upper surface is considered to be the most prominent density boundary by Table 2-7. Therefore the subsurface density structure can be approximated by two-layered structure. The automatic calculations of the two-layered model were applied by using first-order gravity residuals.

Calculations were made for the density contrast ($\Delta\rho$) of 0.3 g/cm^3, 0.5 g/cm^3, 0.7 g/cm^3 and 0.9 g/cm^3. The density difference between the Lower Member of the Jampang Formation and its overlying formations is supposed to range from 0.4 g/cm^3 to 0.8 g/cm^3.

The control points of the analysis were selected on the outcrop of Lower Member of Jampang Formation on the A-C' and B-C profiles. Then the calculated depth of the A-C' and B-C at the profile intersections were used as the control point for the D-E profile. The results of the profile analysis are shown in Figs. 2-15 to 2-17.

(1) A-C' profile (Fig. 2-15)

This profile passes from the gravity high H_1 (Middle Ciwulan uplift) toward the Cibuniasih barite bed through the center of the gravity low L_1 (Cikalong basin) from west to east. The control points were selected at 100 msl of the almost west-end and at 125 msl of the east-end where the basement is exposed.

The basement depth at the center of the Cikalong basin is estimated -470 msl by the density contrast $\Delta\rho$=0.9, -670 msl by $\Delta\rho$=0.7, -1,080 msl by $\Delta\rho$=0.5. Considering the tuff of the Upper Member of the Jampang Formation distribute on the surface here, this low density tuff is supposed to deposit thickly on the basement to near surface. Therefore there is possibility that the density contrast is more than 0.7 g/cm^3 (see Table 2- 7). The depth of the basement is estimated the range from -700 msl to -500 msl.

It is apparent that the western slope of the basin is steep and could be interpreted geologically as faults. The eastern slope, in contrast, is relatively gentle.

(2) B-C profile (Fig. 2-16)

This profile passes from Cisasah Gypsum mine toward the gravity high H_2 (Pasir Gintung uplift) through the center of the gravity low L_3 (Cibongas basin) from northwest to southeast. The control points were selected at 75 msl of the Ciwulan and at 125 msl of the east-end where the basement is exposed.

The basement depth at the center of the Cibongas basin is estimated -360 msl by the density contrast $\Delta\rho$=0.9, -500 msl by $\Delta\rho$=0.7, -790 msl by $\Delta\rho$=0.5. The limestone-calcareous sandstone of the Bentang Formation and the Kalipucang Formation are distributed on the surface here. The thickness of these formation, however, is expected less than 100m. And low density tuff of the Upper Member of the Jampang Formation is supposed to deposit thickly below those. Therefore $\Delta\rho$ is considered to be ranged from 0.5 to 0.8. The depth of the basement is estimated the range from -800 msl to -400 msl.

There are faults from the geological evidence at the east part of this profile. The gravity gradients there is not so steep. It suggests that the displacement of these faults are not so large.

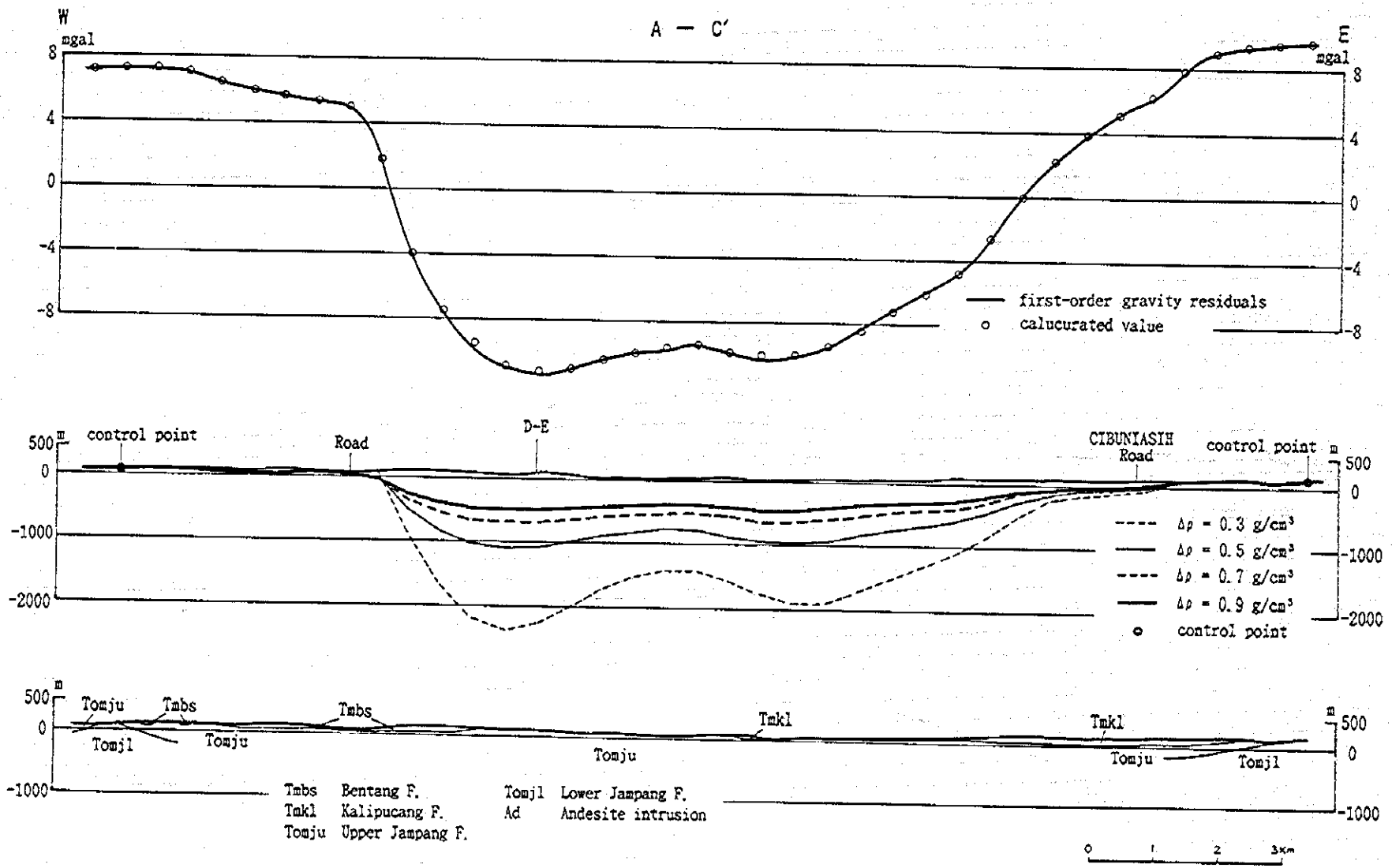

Fig. 2-15 Two-Dimensional Gravity Analysis Profile (A-C')

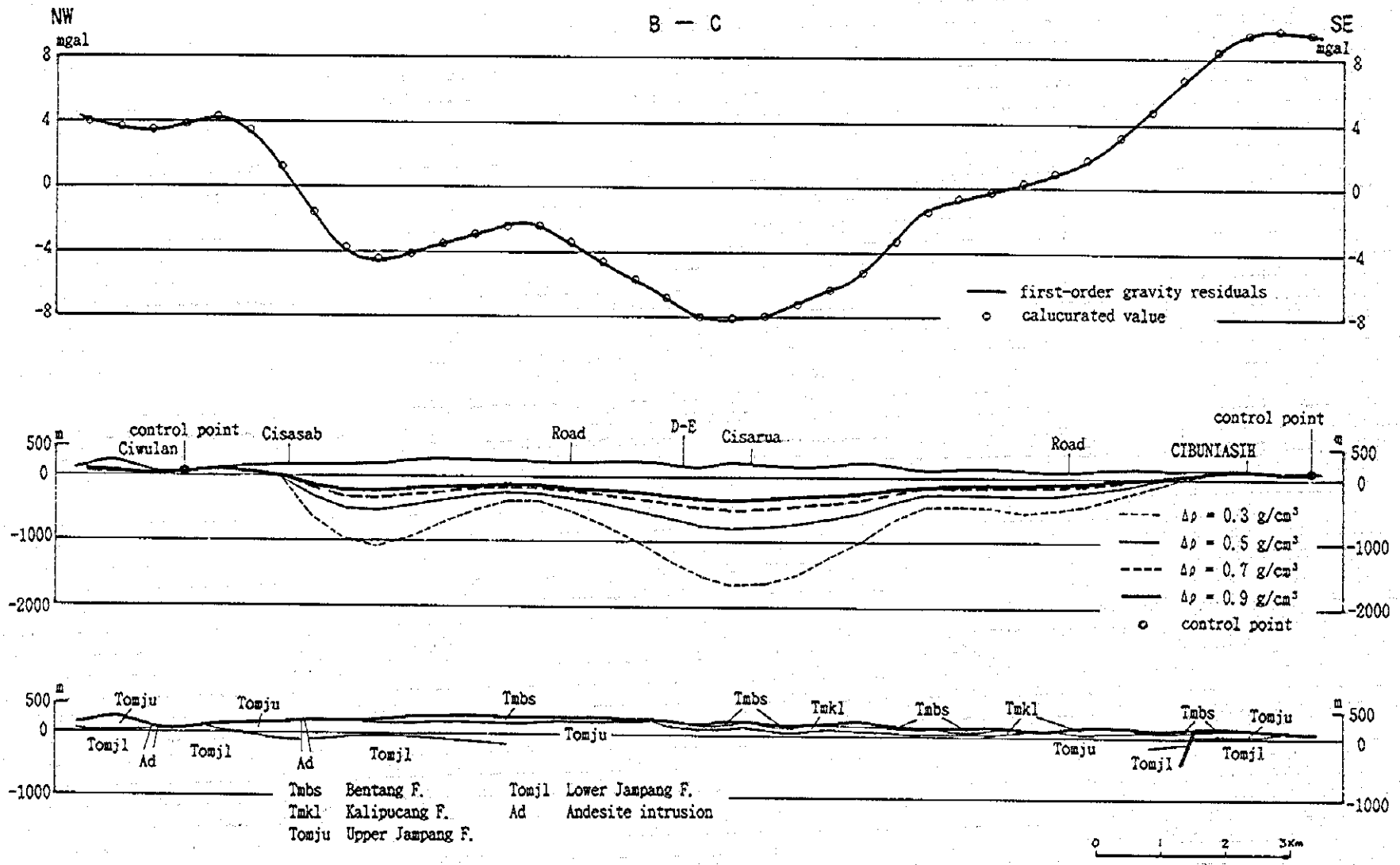

Fig. 2-16 Two-Dimensional Gravity Analysis Profile (B-C)

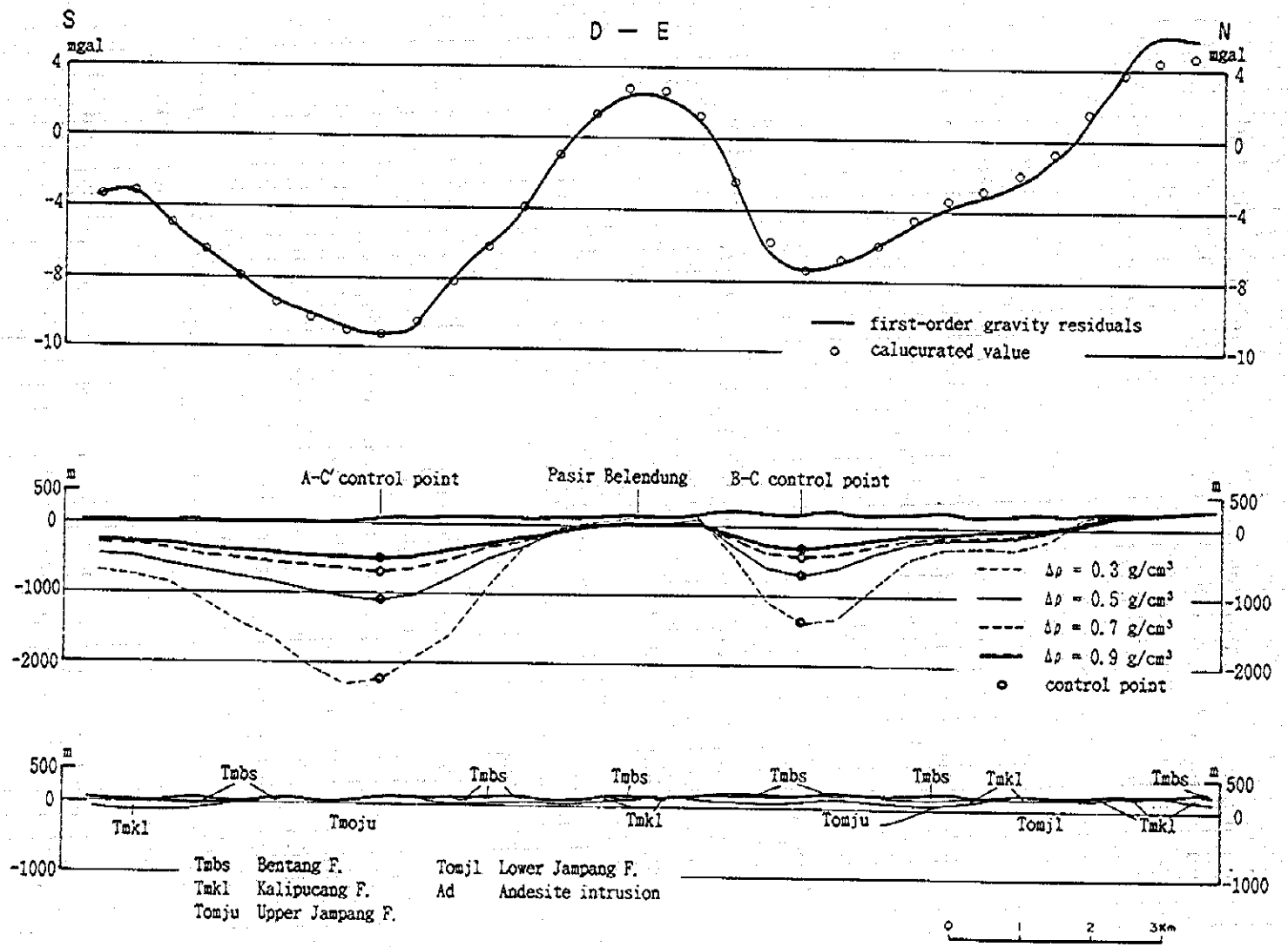

Fig. 2-17 Two-Dimensional Gravity Analysis Profile (D-E)

(2) D-E profile (Fig. 2-17)

This profile passes through the gravity low L_1 (Cikalong basin) from south to north, and continues to the gravity low L_3 (Cibongas basin) then to the gravity high H_3 (Pasir Garu uplift). The control points were selected at the calculated depth of the A-C' and B-C at the profile intersections.

The basement depth at the gravity high which sets apart the Cibongas basin from Cikalong basin is estimated about +30 msl by the density contrast $\Delta\rho$=0.7 and $\Delta\rho$=0.5. The tuff of the Upper Member of the Jampang Formation is supposed to be thin, less than 100m, here.

From the result of the calculation, the basement is expected to expose in the northern end of this profile. It is supported by the fact that the Lower Member of the Jampang Formation is distributed along the river in that area.

3-3 Discussion

As a result of the analysis of the gravity residuals in conjunction with geologic structure of this area, three important structural components -- (1) basin and uplift, (2) fault, and (3) local trough -- were defined.

Following two basins and three uplifts were distinguished in this area.

- Cikalong basin and Cibongas basin
- Middle Ciwulan uplift, Pasir Gintung uplift and Pasir Garu uplift

The Cikalong basin, located from Pasir Nyatu to the lower reaches of Cimedang, is the most remarkable gravity low in the survey area. This basin is about 10 km from east to west and 6 km from north to south. The basement depth is estimated the range from -700 msl to -500 msl from 2-dimensional profile analysis. To it's west, the gravity gradient is steep towards the Cikalong-Cikatomas road, and continues up to the Middle Ciwulan uplift. The eastern slope, in contrast, is relatively gentle. It goes up until the Pasir Gintung uplift. This basin was interpreted to be composed of the green tuff basin probably formed during the middle Miocene Period. At the north of the Cikalong basin, there are three smaller gravity lows arranged in the E-W direction. These were named the Cibongas basin altogether.

The gravity highs - in Pasir Gintung, in the middle reaches of Ciwulan and at Pasir Garu - coincide well with the distribution of the Lower Member of the Jampang Formation. Therefore, they are considered to be the uplifts of the basement.

Several steep gravity gradients, interpreted as steep change of basement depth, were found and considered geologically as faults. Some of them are N-S system: at the

western side of the Cikalong basin, and at the western side of the Pasir Garu uplift. There is other gravity gradients not so steep but interpretable to be faults from the geological evidence at the north of Cibuniasih. Another is E-W system: at the northern side of the Cikalong basin.

A local trough was found in the vicinity of Cibuniasih barite digging on the gravity residuals map. It is located at the flank of the gravity structure between the Pasir Gintung uplift and Cikalong basin, stretching to the southwest. Another trough-like structure was recognized at the south of Cisasah gypsum mine stretching to the northeast.

The known stratabound mineral showings lie on the flank of gravity structure from an uplift to a basin. The Cibuniasih barite bed occurs in a local gravity trough on the flank of the Pasir Gintung uplift to the Cikalong basin. The Cisasah gypsum deposit is situated on the flank from the Middle Ciwulan uplift to the Cibongas basin. The Cidadap gypsum deposit, which is not so distinctive as the former two cases, looks to be located at the middle of the Middle Ciwulan uplift down to a gravity low near the coast of Indian Ocean. The local trough structure of green tuff which occurs on the flank from a basement uplift to a basin seems to provide favorable loci for the deposition and preservation of massive sulfide deposit.

Another interesting feature from the gravity geophysical point of views is the spatial relationship of manganese ores to gypsum or barite ores. The stratabound manganese ores occur near the gypsum or barite, and always occupy structurally at a higher position to them.

Chapter 4 IP Electric Survey

4-1 Outline of the Survey

Time-domain IP (Induced Polarization) survey was carried out in the Cibuniasih-Balekambang area (shown in Fig. 1-2) which was extracted by the preceding geological, geochemical and gravity survey. The objective of the survey is to clarify the electric characteristics of the subsurface zones and thus to detect IP anomalies related to mineralization of this prospective area.

Field measurement was done for the total 23.2 km of 12 survey lines shown in Fig. 2-18. The dipole-dipole array configuration (with 50m electrode spacing; N=1,2,3,4,5; 0.25 Hz) was applied. Resistivity and chargeability of 26 selected samples were measured in the laboratory.

4-2 Survey Method

4-2-1 Methodology

The IP method is the exploration method to observe electric polarization effect (IP effect) in the earth. The IP effect is caused by the following phenomena.

When the direct current flows through the rocks containing metallic minerals, electric potential difference is generated between the surface of metallic minerals and pore water around it. Electric charge is stored and therefore electric polarization is resulted in. After the current is switched off, this electric charge is discharged gradually. It forms the residual voltage decaying with passage of time. However this IP effect also occurred in sedimentary rocks containing clay.

For the time-domain IP survey, on and off alternating rectangular wave (Fig. 2-19) is used as transmitter current. Received voltage is as shown also in Fig. 2-19. It is composed of the primary voltage Vp observed while current is on and the decay voltage Vs while current is off. The chargeability M, shown in equation (4-1), is commonly used as index to express quantity of IP effect.

$$M = \frac{1}{Vp} \int_{t_2}^{t_1} Vs \, dt \qquad (4\text{-}1)$$

It is the proportion of time integral of secondary voltage to primary voltage. Its unit is mV-S/V (milli-seconds).

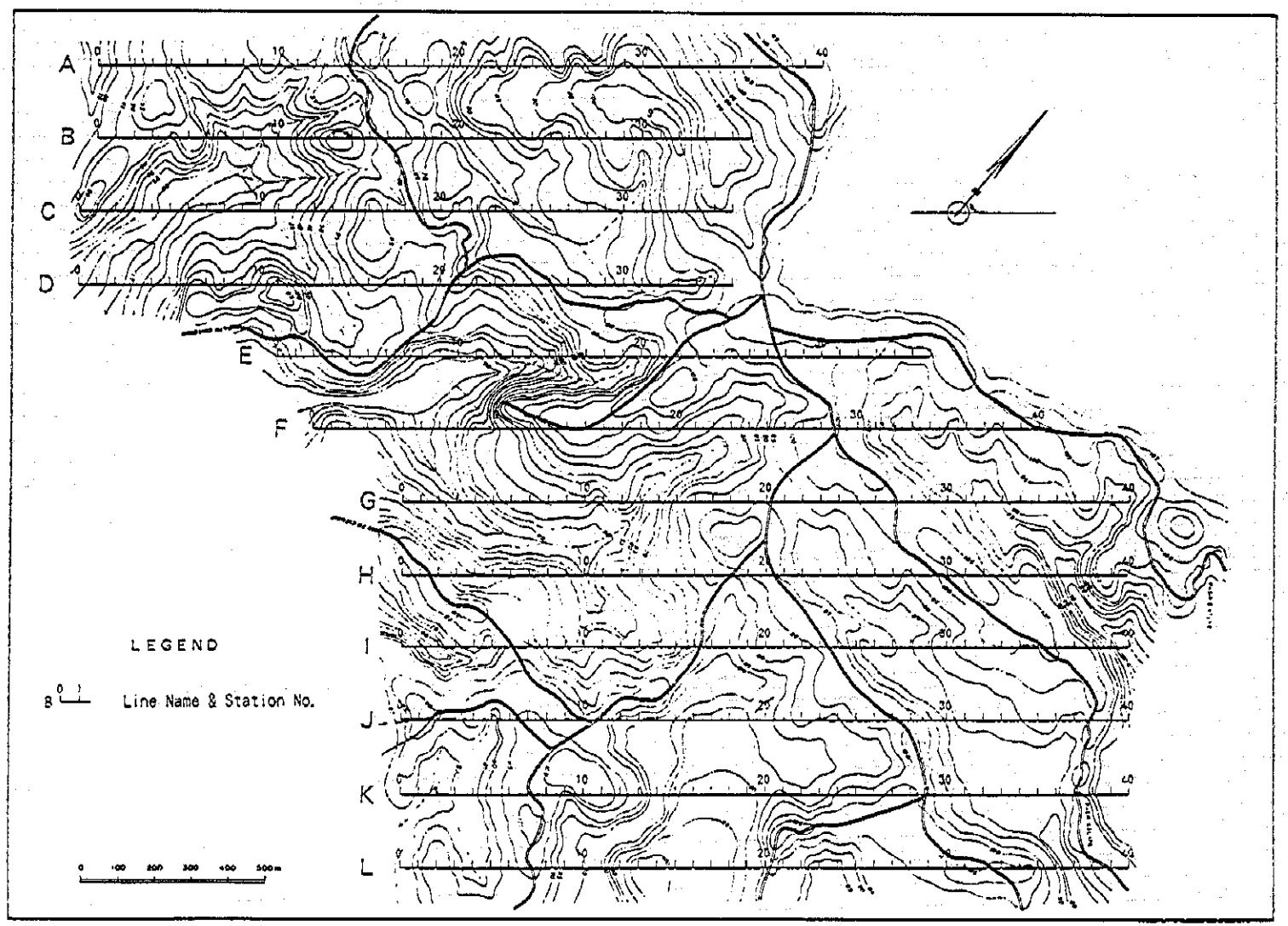

Fig. 2-18 Location Map of IP Survey Lines

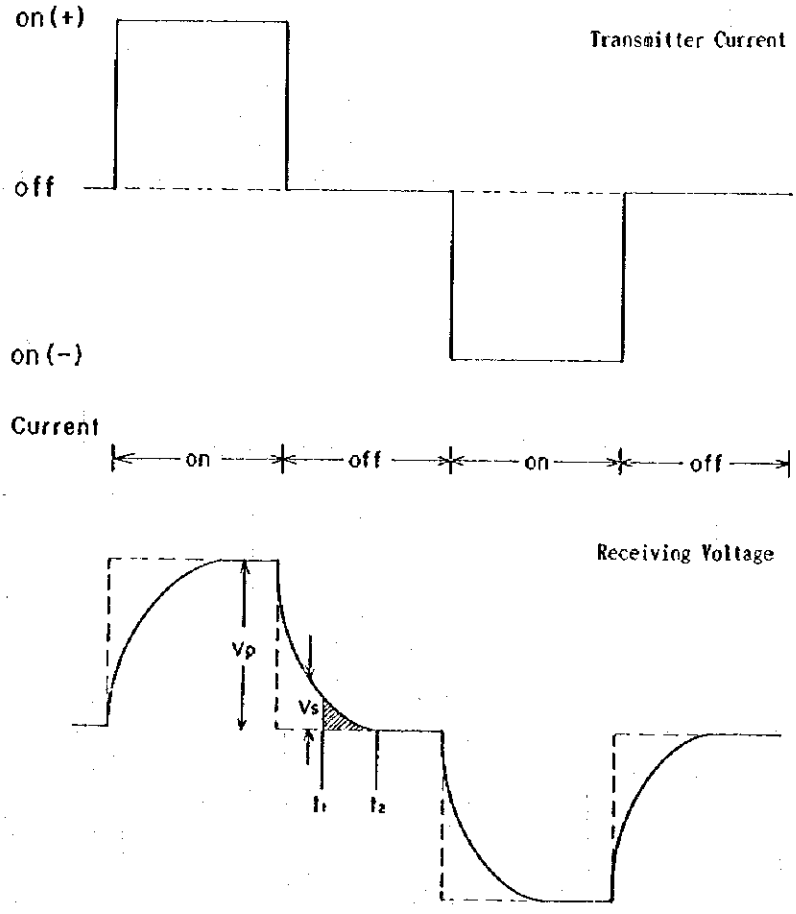

Fig. 2-19 Time-Domain IP Wave Form

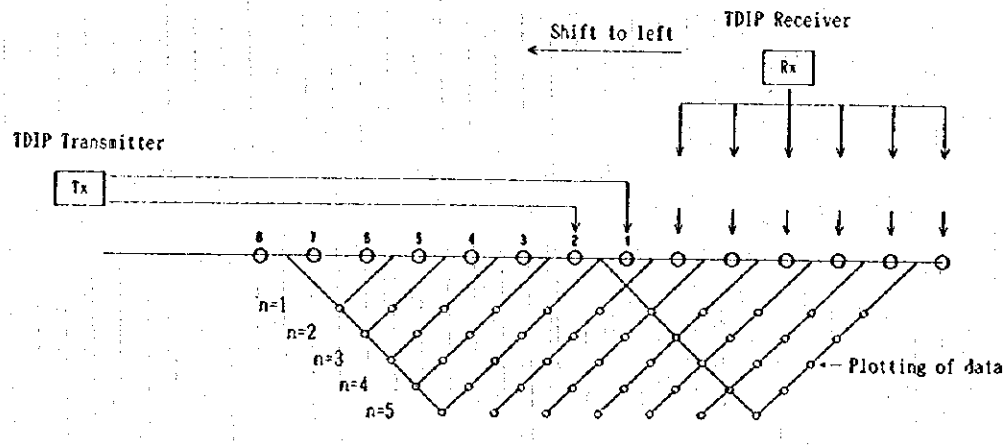

Fig. 2-20 Illustration of IP Measurement

4-2-2 Field Survey

(1) Survey lines

Total 23.2 km (12 lines) were set in the area. The location of IP survey lines is already shown in Fig. 2-18. The line intervals were 200 m. It is relatively long in order to cover the whole prospective area with limited line length. Open traverse leveling was done by Wild transit . Summary of each line is as follows.

Line	Length (m)	Points of measurement
A	2,000	180
B	1,800	160
C	1,800	160
D	1,800	160
E	1,800	160
F	2,000	180
G	2,000	180
H	2,000	180
I	2,000	180
J	2,000	180
K	2,000	180
L	2,000	180
TOTAL	23,200	2,080

(2) Instrumentation

The equipment used in this survey is as follows:

(a) Receiver : Zonge GDP-16 data processor
8 channels, current on/off cycle 0.001 to 1 Hz
Automatic cancellation of self potential.
Preset 13 windows and automatic measuring and data storage in the semiconductor memory data.

(b) Transmitter :

	Zonge GGT-5	Zonge GGT-10
Output voltage	250 - 1000 V	50 - 1000 V
output current	0.2 - 25 Amp.	0.2 - 20 Amp.
frequency range	0.125 - 2,048 Hz	DC - 8 kHz

(c) Transmitter controller : Zonge XMT-16
Frequency range DC - 8,192 Hz

(d) Generator : Zonge ZMG-5
Output power 5 kw, output voltage 115 volts, frequency 400 Hz, engine 5 HP 4 cycle.

(f) Electrode : transmitting dipole stainless rods (length 50 cm)
receiving dipole porous pot with Cu-$CuSO_4$

(3) Measurement

The specification of IP survey is as follows :

configuration of electrode array : dipole-dipole
separation of electrode : 50 m
coefficient of electrode separation : N=1,2,3,4,5
the duty cycle of on/off cycle : 0.25 Hz

Receiving dipoles and transmitting dipole were set on the survey line as shown in Fig. 2-20.

The chargeability of GDP-16 is defined in the following calculations :

$$M = T/1024 \times 1.87 / Vp \times \int Vs \qquad (mV\text{-}S / V) \qquad (4\text{-}2)$$

Where (at 0.25 Hz)

T : cycle period of 4 second

1024 : sampled points per cycle

1.87 : Newmont constant

Vp : primary voltage of the respective dipole

$\int$Vs : the integral of decay voltage from 0.5 sec to 1.1 sec

This value will be slightly lower than the Newmont Standard chargeability.

The apparent resistivity (AR) is defined as :

$$AR = \pi\, an(n+1)(n+2)\, Vp/I \qquad (ohm\text{-}m) \qquad (4\text{-}3)$$

a : interval of the respective dipole

n : coefficient of dipole - dipole

Vp : primary voltage of the respective dipole

I : transmitter current

4-2-3 Laboratory Test

Resistivity and chargeability of 26 rock and ore samples in the survey area were measured in laboratory in Japan. The same method and instrument as field measurement was used.

4-2-4 Analytical Method

The measured resistivity and chargeability values are shown on the profiles of each line. They are also shown on the plane maps of each depth by the electrode separation index. The subsurface electric characteristics can be understood from these plane maps and profiles.

Two-dimensional model simulation was carried out for IP anomalies, and chargeability and resistivity values were obtained quantitatively for the anomaly sources.

4-3 Survey Results

4-3-1 Apparent Resistivity

The measured apparent resistivity values are laid out for each line in Figs. 2-21 and 2-22. These values are also shown on plane maps for three depths by electrode separation index N=1,3,5 in Figs. 2-23, 2-24 and 2-25. These maps approximately coincide to the one for the depths of 50m, 100m, 150m below surface.

The characteristics of the apparent resistivity of this area are as follows.

- The resistivity values are predominantly low in the range from 5 to 30 ohm-m.

- Relatively high resistivity values (>30 ohm-m) from shallow to deep subsurface zones are detected in the south-eastern part of the survey area (lines K, L and south-western part of line J) where the basement is expected shallower by preceding gravity survey and also detected at Nos. 6-16 of line A. Relatively high resistivity values in shallow zones are detected in the small part of lines B, C ,D and H. These are effects of high resistivity limestone of the Kalipucang Formation on the surface in lines B, C and D.

- Very low resistivity (<10 ohm-m) is detected widely in the central parts of the survey area from shallow to deep zones (lines D, E, F and part of lines C, G, H). This area coincides the trough of gravity structure.

4-3-2 Chargeability

The measured chargeability values are shown for each line in Figs. 2-26 and 2-27. These values are also shown on the plane maps for three depths by electrode separation index N=1, 3, 5 in Figs. 2-28, 2-29 and 2-30. These map approximately coincide to the one for the depths of 50 m, 100 m, 150 m below surface.

The characteristics of the chargeability are as follows.

The chargeability values are predominantly low. The average is 2.5 mV·S/V and the standard deviation is 1.1 mV·S/V. But this background value is higher in the western part of the survey area. (line A and the south-western part of lines B, C, D). In this area, lime stone is distributed on the surface.

Chargeability more than 4.0 mV·S/V is defined as anomaly. Anomalies are mainly detected at following three area.

(a) the south-western part of lines C and D (located in Sukasari)

These anomalies occur from middle into deep zones in the very low resistivity background (<10 ohm-m). They have not much difference in resistivity values from the low background.

(b) the south-western part of line A (located in Sukasari)

These anomalies are detected from shallow into deep zones in the relative complex resistivity pattern due to the limestone hill on the surface. They have not much difference in resistivity from the background ranged from 10 to 30 ohm-m.

(c) the middle part of lines J, K and L (located in Bihbul)

These anomalies occur from shallow into deep zones at the margin of relative high resistivity (>30 ohm-m) area.

Groups of shallower and smaller scale anomalies extends in E-W direction in right handed echelon like arrangement from anomalies (c). These are :

- in the vicinity of Nos. 11 and 16 on line I
- in the vicinity of No. 8 on line H

Other small anomalies occur at the vicinity of No. 5 on line E and No. 36 on line A.

4-3-3 Laboratory Test

Resistivity and chargeability were measured for 26 samples collected from the surface and drilling core in the laboratory with the field equipment under field conditions. The results are shown in Table 2-8 and the average values are as follows.

Rock	Resistivity(ohm-m)	Chargeability(mV·S/V)
Tuff (U.Jampang F.)	25	7.3
Sandstone(Kalipucang F.)	22	11.3
Gypsum	910	1.6
Manganese ore	54	144
Siliceous ore (Py,Cp imp)	660	126

Table 2-8 Chargeability and Resistivity in Laboratory

No.	Rock Name	Deeps (m)	Chargeability (mv/v)	ρ (Ω·m)	Remarks
1	Gypsum	Surface	1.7	518	
2	Gypsum	Surface	1.5	1,980	
3	Gypsum	Surface	1.7	240	
4	Manganese ore	Surface	143.9	54	
5	Siliceous ore	Surface	80.1	1,590	Py, Cp, imp
6	Siliceous ore	Surface	112.7	310	Py, imp
7	Siliceous ore	Surface	185.9	88	Py, Cp, imp
8	Sand stone	MIT-5 5.25	17.6	33	
9	Sand stone	MIT-5 5.40	5.4	12	
10	Fine tuff	MIT-5 28.50	9.7	43	
11	Fine tuff	MIT-5 28.70	7.0	60	
12	Fine tuff	MIT-5 28.90	3.1	41	
13	Dacitic tuff	MIT-5 38.75	8.0	31	
14	Dacitic tuff	MIT-5 38.85	8.1	10	
15	Coarse tuff (sandy)	MIT-5 56.05	12.2	16	
16	Coarse tuff (sandy)	MIT-5 56.15	15.1	16	
17	Coarse tuff (sandy)	MIT-5 56.25	1.7	16	
18	Coarse tuff (sandy)	MIT-5 106.36	4.7	42	
19	Coarse tuff (sandy)	MIT-5 106.45	8.3	39	
20	Coarse tuff (sandy)	MIT-5 106.50	2.5	26	
21	Coarse tuff (sandy)	MIT-5 124.96	7.7	18	
22	Coarse tuff (sandy)	MIT-5 125.05	4.6	17	
23	Coarse tuff (sandy)	MIT-5 128.80	7.0	10	
24	Coarse tuff (sandy)	MIT-5 129.00	4.6	11	
25	Coarse tuff (sandy)	MIT-5 129.10	5.2	10	
26	Coarse tuff (sandy)	MIT-5 141.20	14.5	12	

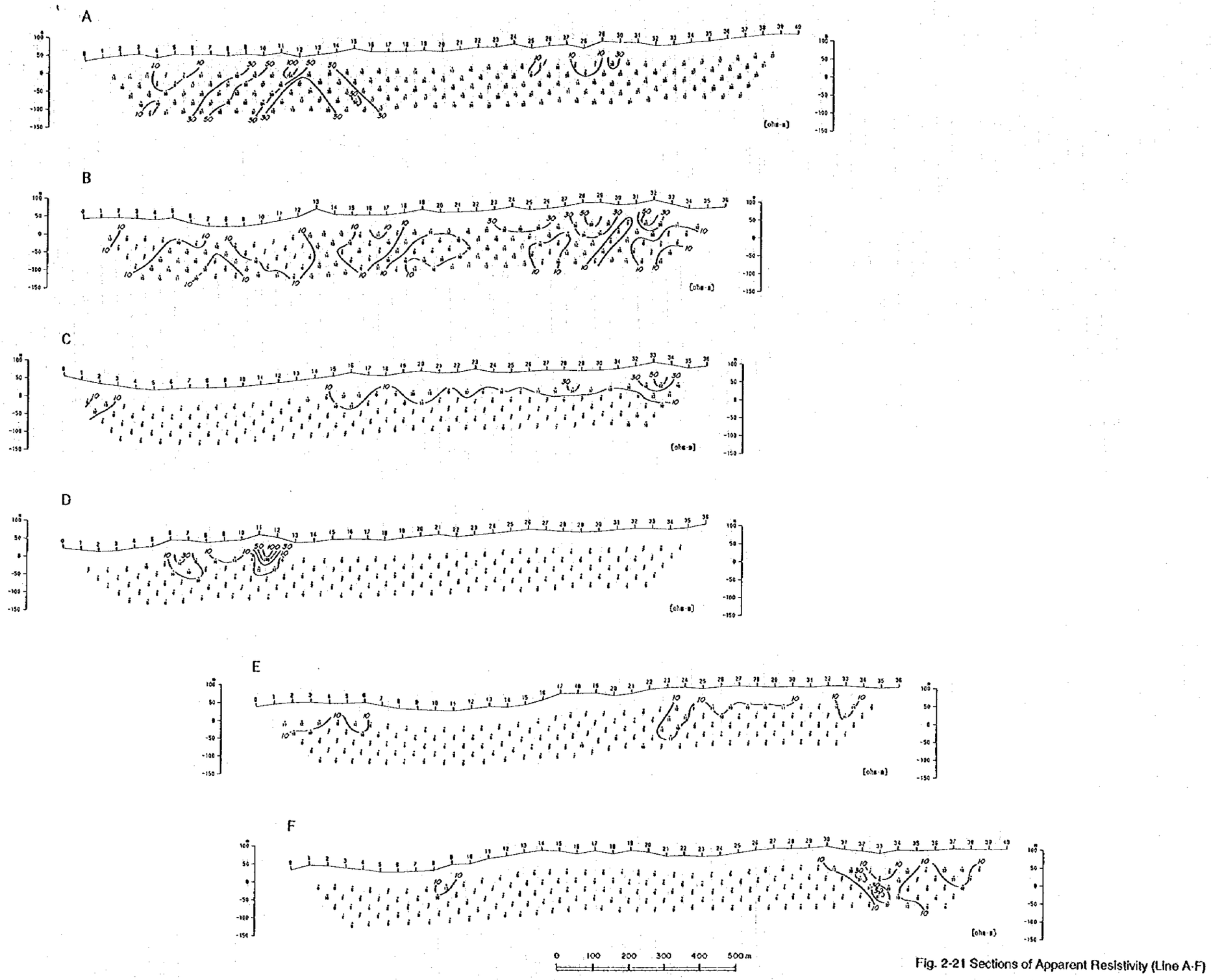

Fig. 2-21 Sections of Apparent Resistivity (Line A-F)

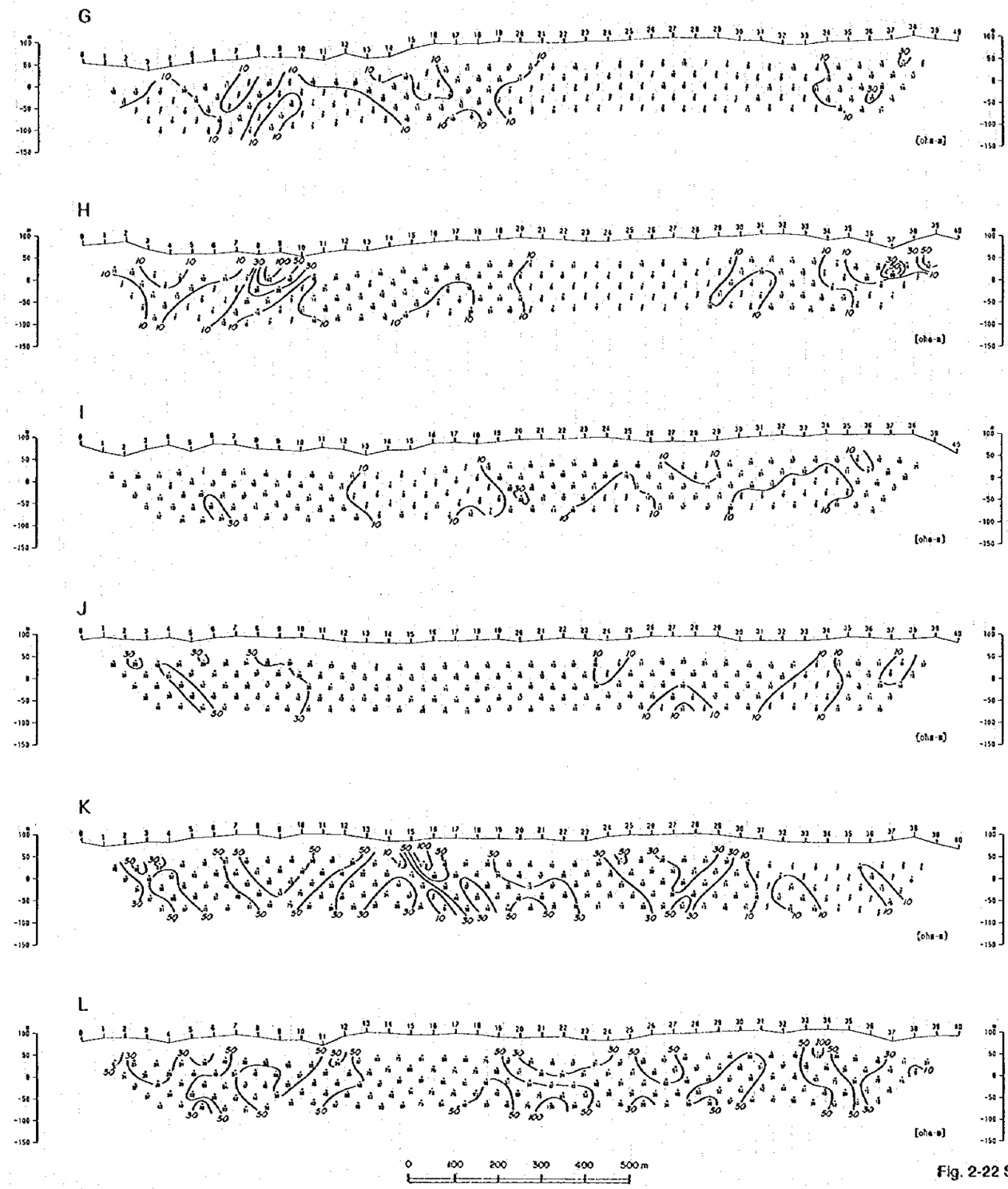

Fig. 2-22 Sections of Apparent Resistivity (Line G-L)

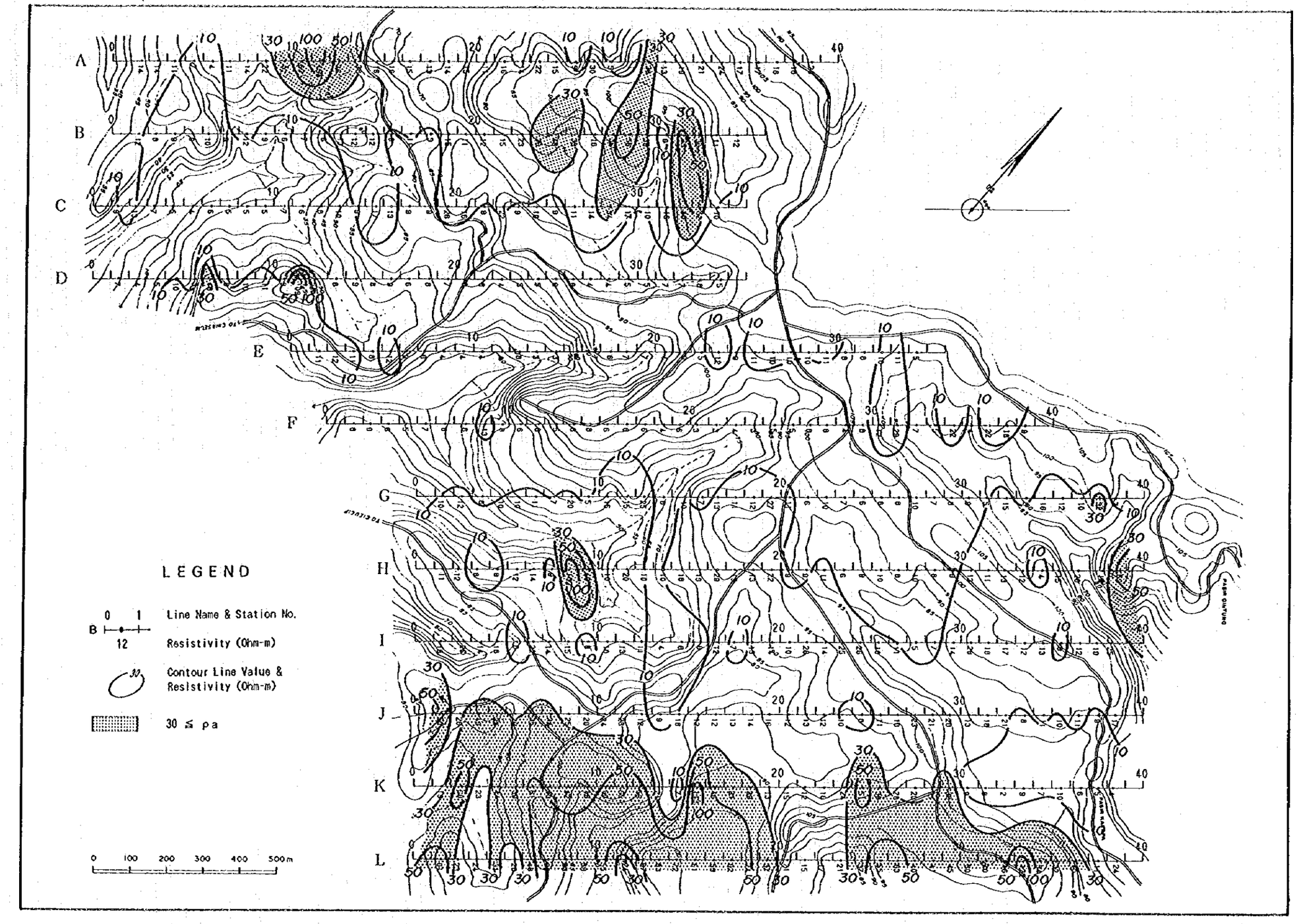

Fig. 2-23 Plan Map of Apparent Resistivity (N=1)

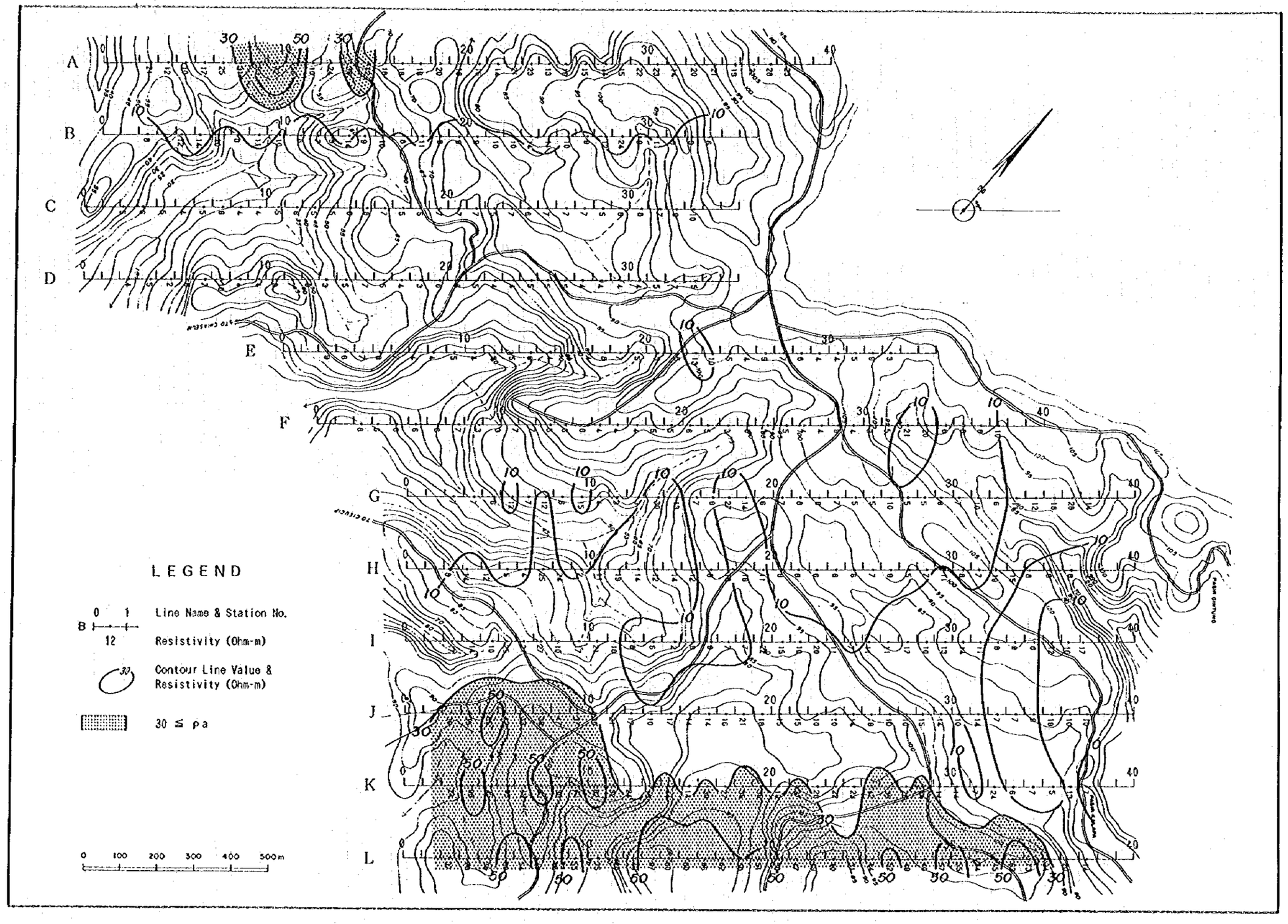

Fig. 2-24 Plan Map of Apparent Resistivity (N=3)

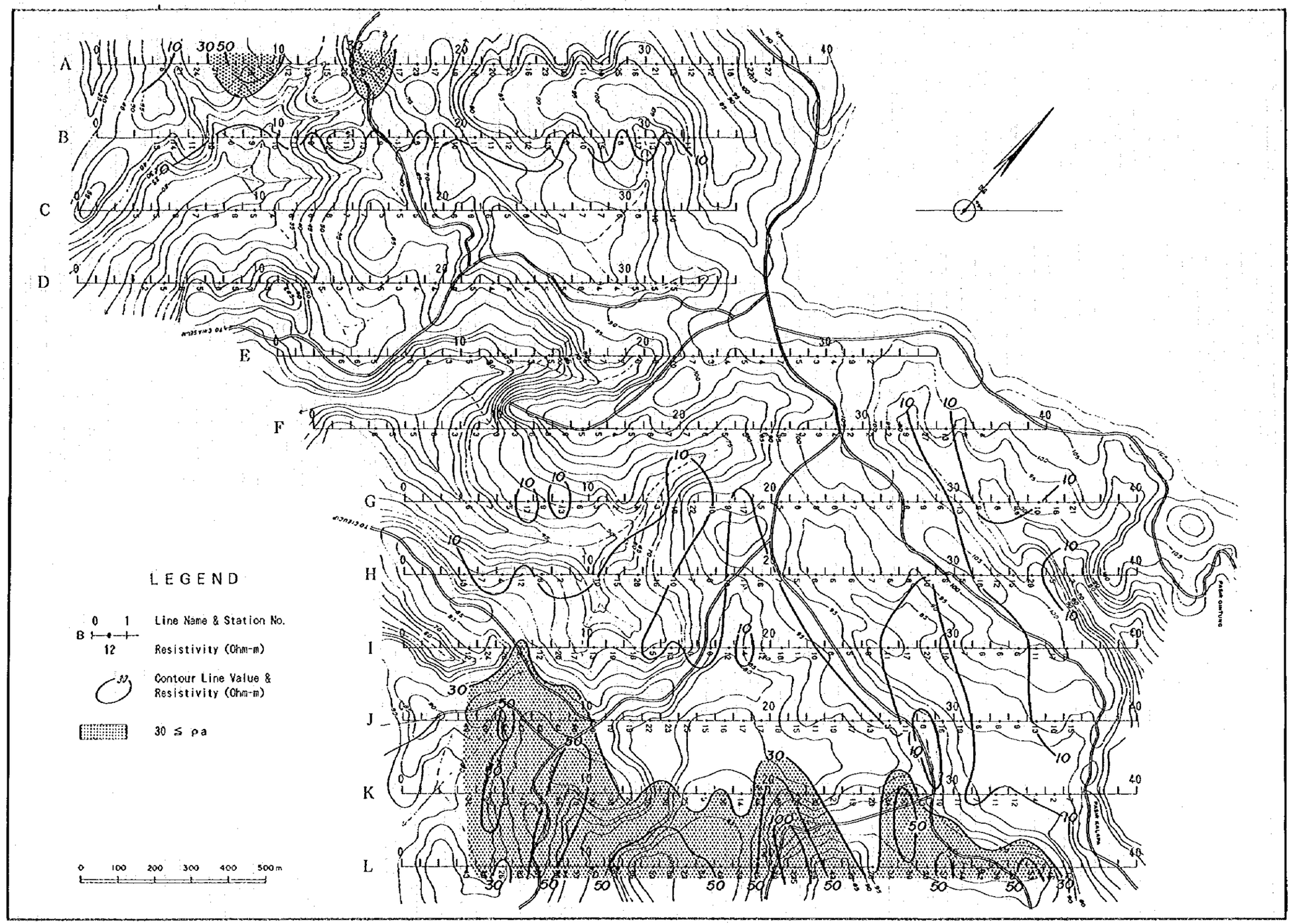

Fig. 2-25 Plan Map of Apparent Resistivity (N=5)

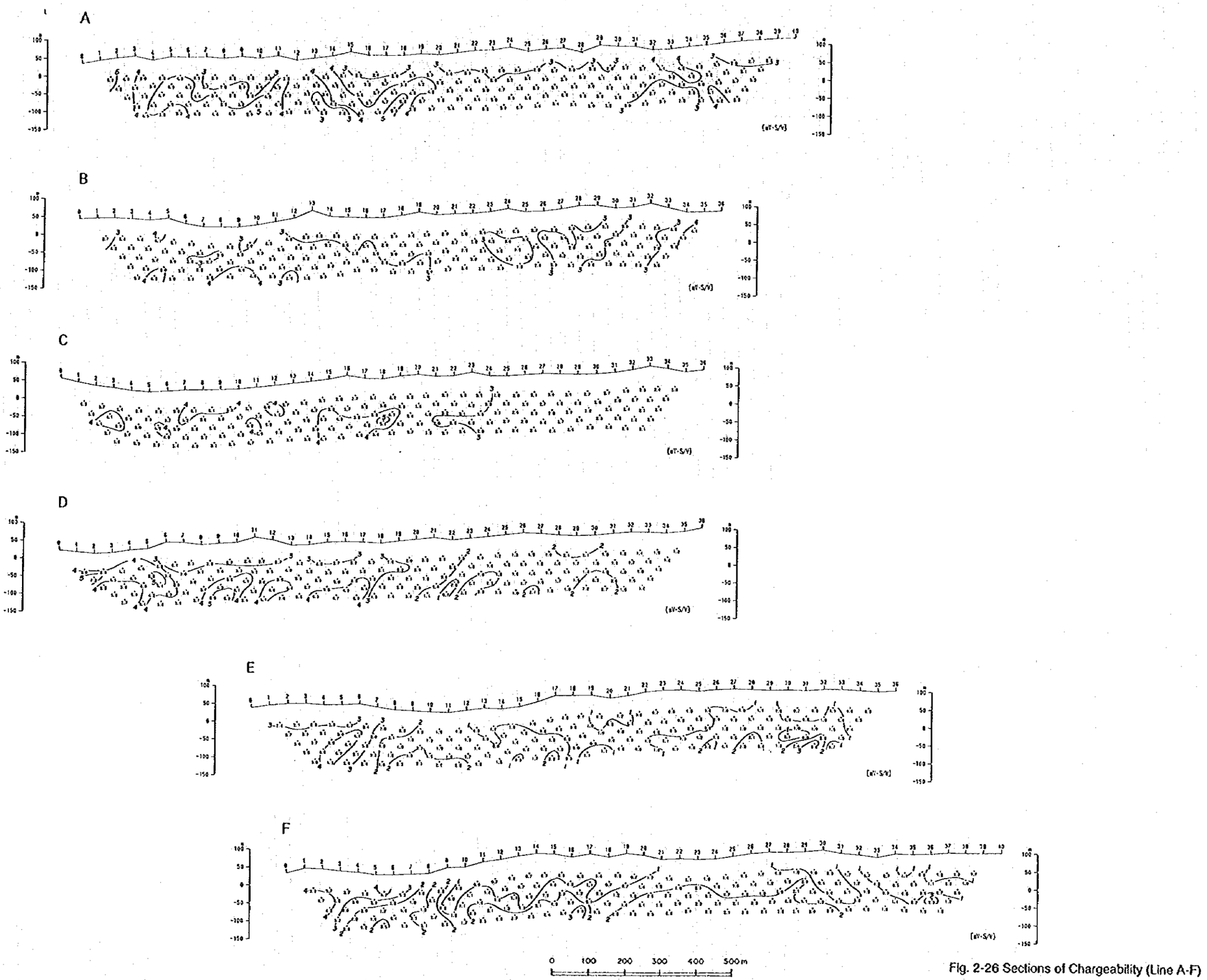

Fig. 2-26 Sections of Chargeability (Line A-F)

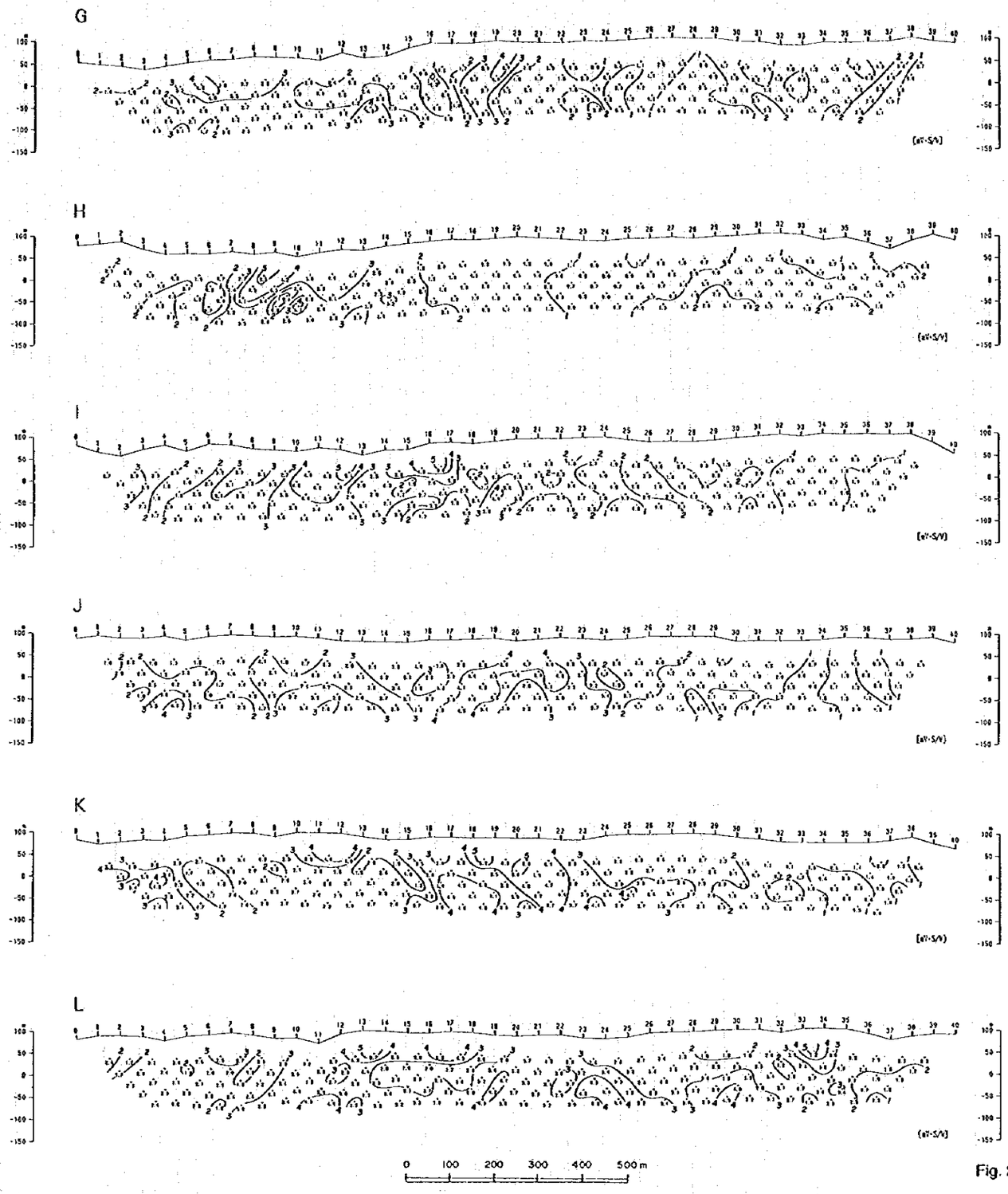

Fig. 2-27 Sections of Chargeability (Line G-L)

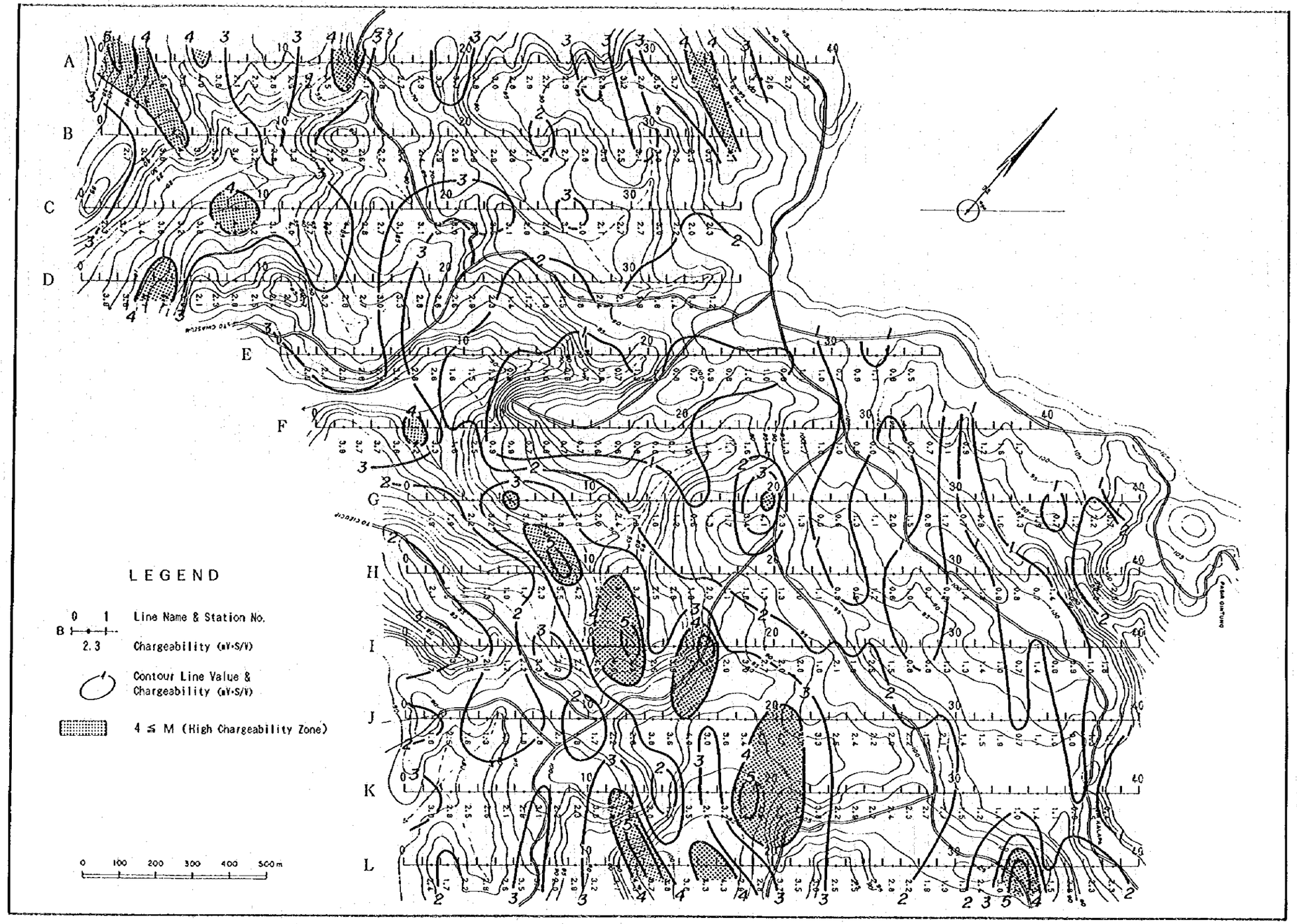

Fig. 2-28 Plan Map of Chargeability (N=1)

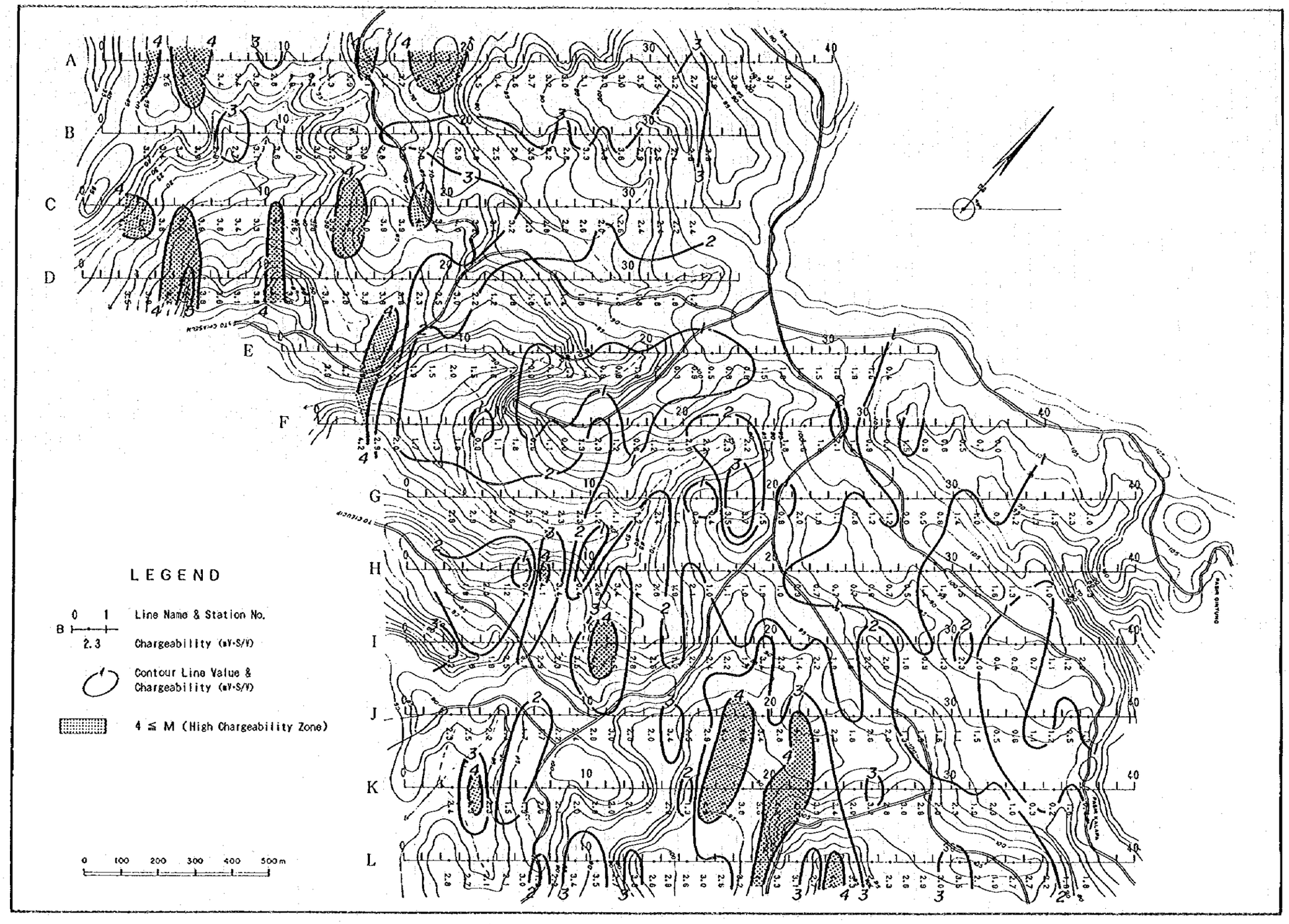

Fig. 2-29 Plan Map of Chargeability (N=3)

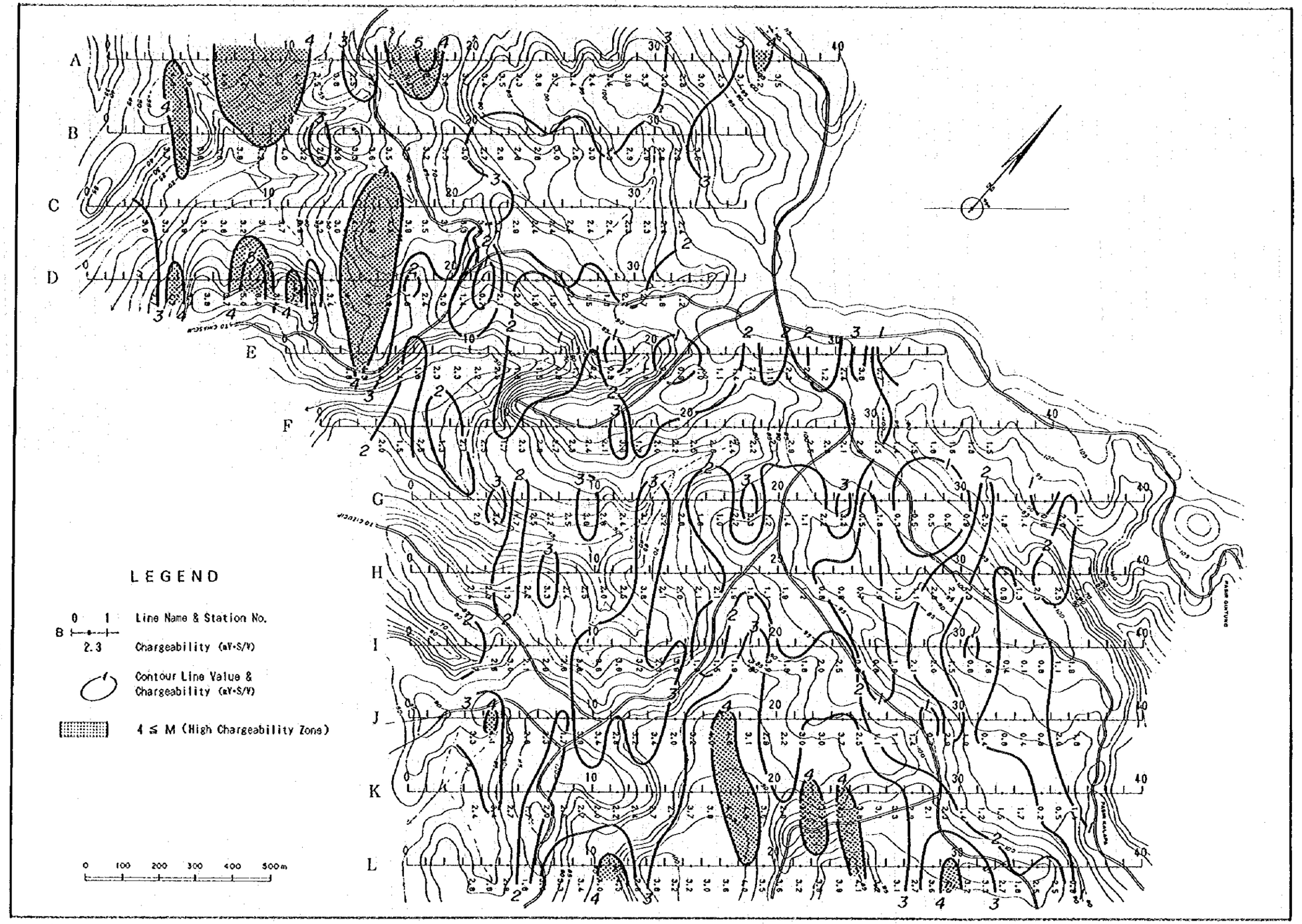

Fig. 2-30 Plan Map of Chargeability (N=5)

The resistivity of tuff, sandstone and manganese ore is low and of gypsum and siliceous ore is high. Tuff of the Upper Member of the Jampang Formation which corresponds to the background value of this survey is remarkably low. The rock samples in the laboratory have no weak parts such as weathering zones and fracture zones that is high conductive. Consequently, their resistivity in the laboratory is generally measured higher than that of under the ground. These results support the predominantly low resistivity ranged from 5 to 30 ohm-m measured in the field survey.

The chargeability is high in siliceous ore with pyrite and chalcopyrite dissemination, low in tuff and sandstone, very low in gypsum. The average value of 7.3 mV·S/V for tuff is higher than the average chargeability 2.5 mV·S/V in the field survey. The high chargeability of manganese ore is questionable.

4-3-4 Model Simulation Analysis

Two-dimensional model simulation was carried out for three lines, the south-western part of Lines A and D and the central part of line K, where high chargeability anomalies(>4 mV·S/V) are detected. Background was set to 7–40 ohm-m in resistivity and 2.5–3.0 mV·S/V in chargeability. These values correspond to those of the tuff of the Upper member of the Jampang Formation. Assuming mineralized zones were set as similar values as background in resistivity. And its chargeability was supposed to be 30–40 mV·S/V that is about ten times of back ground considering from the laboratory measurement.

Line A (Fig. 2-31)

The high chargeability below Nos. 1–3, 4–11 and 14–19, the high resistivity below Nos. 8–13 were detected in this line. The high chargeability anomalies below the vicinity of No. 10 were also detected in the adjacent line B in the deep zone.

In the model, three high chargeability zones of 30 mV·S/V were set below Nos. 5, 10 and 18 (code 4), and a relatively high chargeability part of 10 mV·S/V was set in the shallow zone below No. 13(code 5). High resistivity and low chargeability was put on the surface of Nos. 3, 11, 15, 19 and 21 assuming limestone hills. Low resistivity and low chargeability zones were set on the rest of the surface corresponding to the sandstone of the Kalipucang Formation.

The results of the simulation are harmonious with the measured results and thus it is considered to be a reasonable model. As the source of the anomaly, the high chargeability zone (30 mV·S/V) with several-tens-meter-scale is supposed to exist in about 150 m below No. 11. The inclined high chargeability layer (about 20 m by 100 m-scale) below No. 5 and the one (about 20 m by 150 m-scale) below No. 18 are supposed to exist in about 100 m below the surface.

Line D (Fig. 2-32)

In this line, the high chargeability below Nos. 2-6, 8-13 and 14-17 and the high resistivity below Nos. 6 and 11 are detected. The high chargeability anomaly below Nos. 14-17 is also detected in the adjacent lines C and E in the deep zone. The anomaly in the deep zone below No. 10 is one of the strongest in this survey.

In the model, two high chargeability zones of 30-40 mV·S/V were set below Nos. 10 and 16 (codes 4, 6), and a relatively high chargeability part of 8 mV·S/V was set in the shallow zone below No. 5 (code 5). High resistivity and low chargeability was put on the surface of Nos. 6 and 16 assuming limestone hills.

The results of the simulation are harmonious with the measured results and thus it is considered to be a reasonable model. As the source of the anomaly, the high chargeability zones (30 -40 mV·S/V) with several-tens-meter-scale are supposed to exist in about 150 m below Nos. 10 and 16. And the relatively high chargeability layer (about 20 m by 300 m-scale) below Nos. 3 -7 are supposed to exist in about 50m below the surface.

Line K (Fig. 2-33)

The high chargeability below Nos. 12 and 16-23, the high resistivity with complex resistivity pattern below the vicinity of No. 15 were detected in this line. The high chargeability anomalies below the vicinity of No. 20 was also detected in the adjacent line J in the shallow zone.

In the model, a high chargeability zone of 35 mV·S/V was set below No. 8 (code 7) and a relatively high chargeability part of 6-7 mV·S/V was set below No. 20 (codes 5, 6). A relatively high chargeability part of 15 mV·S/V was also set below No. 26 (code 9). High resistivity and relatively high chargeability was put on the near-surface of Nos. 12, and 15 (code 4). Low resistivity and low chargeability zone was set on the surface of No. 14. The basement was assumed at about 200m below the surface.

The results of the simulation are harmonious with the measured results and thus it is considered to be a reasonable model. As the source of the anomaly, the relatively high chargeability layer (6-7 mV·S/V) with about 30 m by 150 m-scale are supposed to exist in about 20m below Nos. 18-22. The high chargeability zone (35 mV·S/V) with several-tens-meter-scale may exist in about 150 m below No. 18. Because of the existence of the shallow high chargeability layer, however, mentioned above, accurate interpretation of the deeper part is difficult. Another relatively high chargeability layer (15 mV·S/V) with about 20 m by 150 m-scale are supposed to exist in about 100 m below No 26.

SIMULATION MODEL LINE A

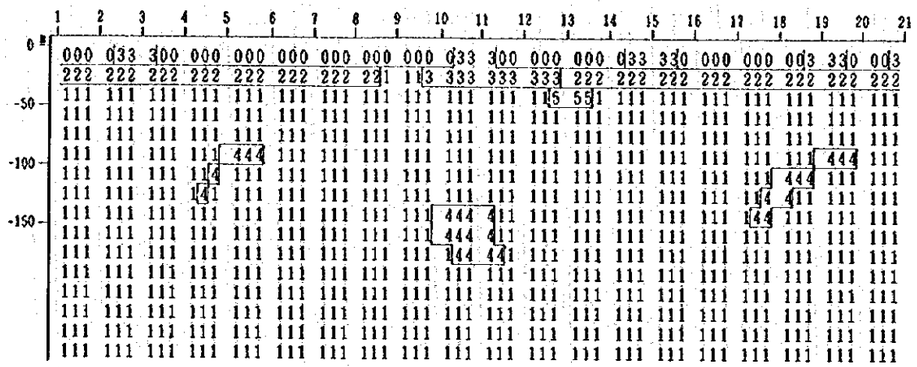

CODE	RESISTIVITY (obm-m)	CHARGEABILITY (mV·S/V)
0	air	
1	30	3.0
2	10	3.0
3	500	3.0
4	30	30.0
5	30	10.0

APPARENT RESISTIVITY

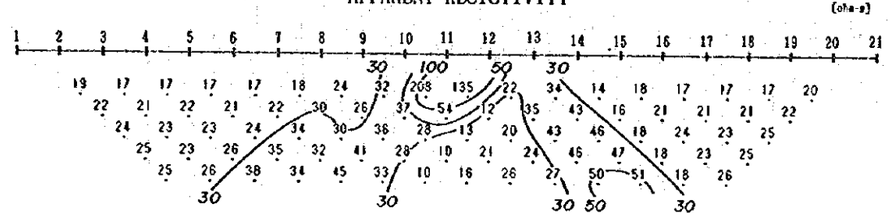

OBSERVED APPARENT RESISTIVITY

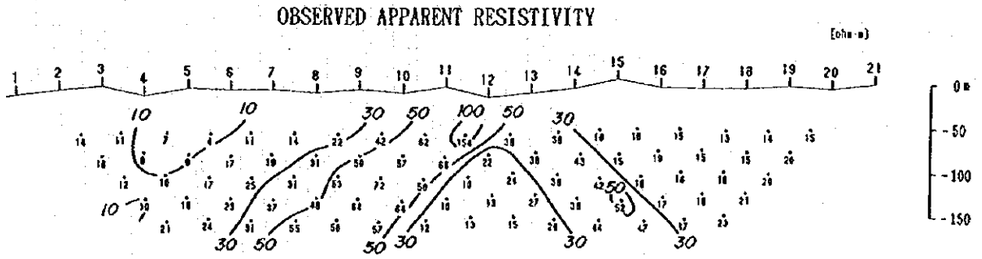

CHARGEABILITY

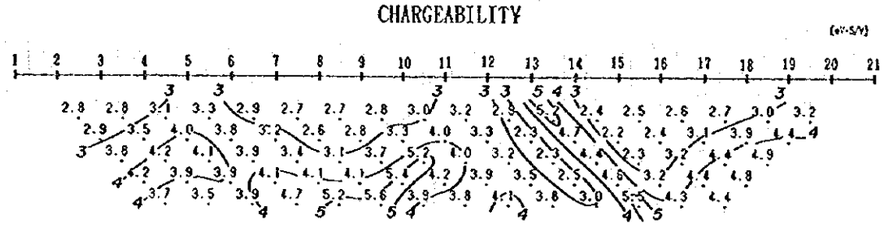

OBSERVED CHARGEABILITY

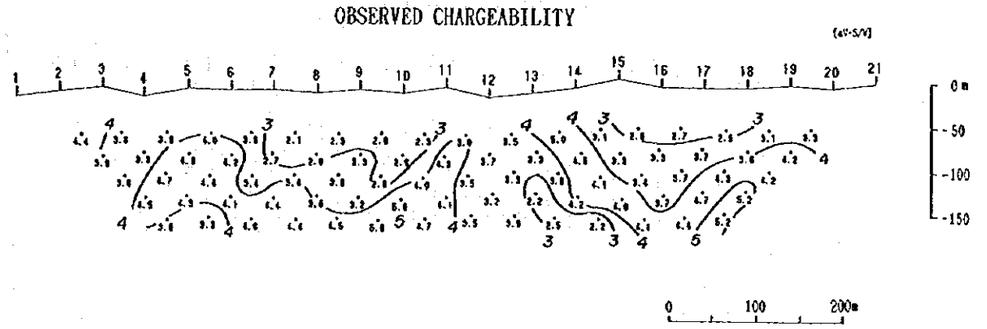

Fig. 2-31 Results of Two-Dimensional Model Simulation (Line A)

SIMULATION MODEL LINE D

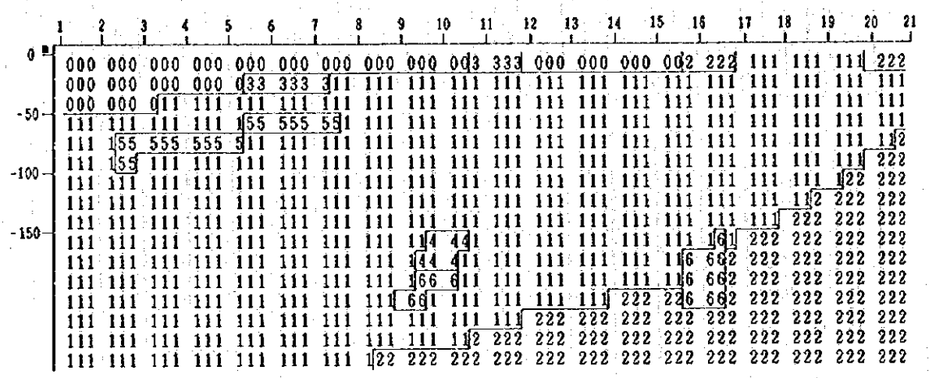

CODE	RESISTIVITY (ohm-m)	CHARGEABILITY (mV·S/V)
0	air	
1	7	3.0
2	7	1.0
3	500	2.0
4	5	30.0
5	5	8.0
6	5	40.0

APPARENT RESISTIVITY

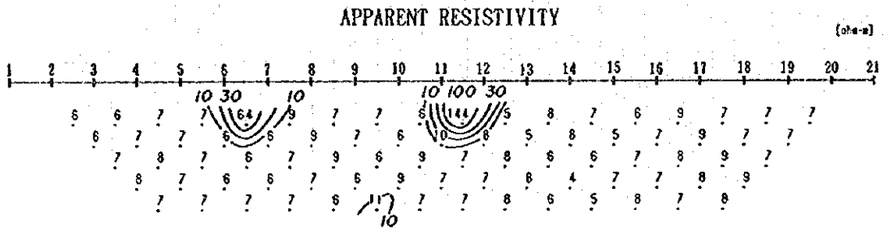

OBSERVED APPARENT RESISTIVITY

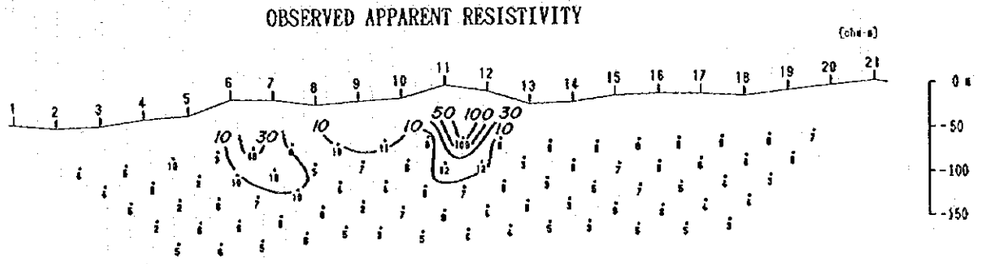

CHARGEABILITY

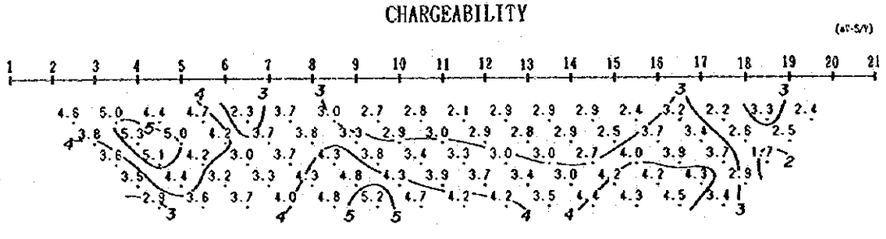

OBSERVED CHARGEABILITY

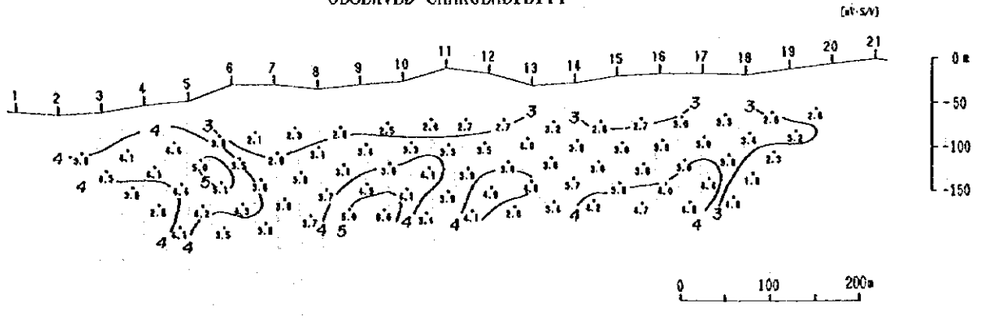

Fig. 2-32 Results of Two-Dimensional Model Simulation (Line D)

SIMULATION MODEL LINE K

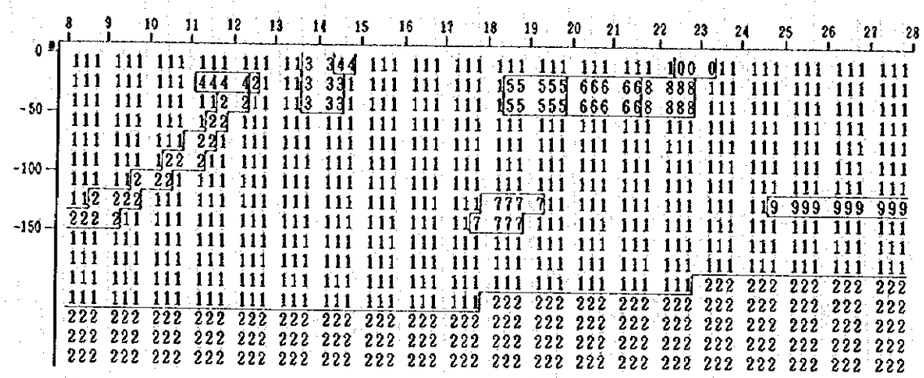

CODE	RESISTIVITY (ohm-m)	CHARGEABILITY (mV·S/V)
0	air	
1	40	2.5
2	300	2.5
3	5	0.5
4	500	8.0
5	15	6.0
6	30	7.0
7	50	35.0
8	20	2.5
9	40	15.0

APPARENT RESISTIVITY

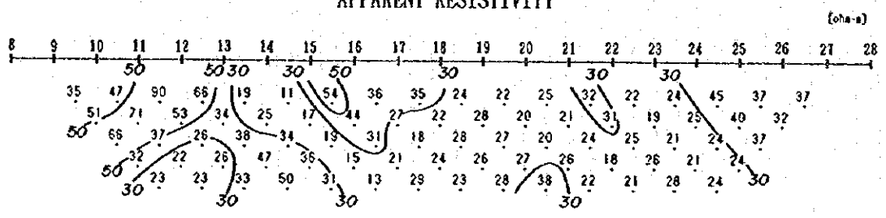

OBSERVED APPARENT RESISTIVITY

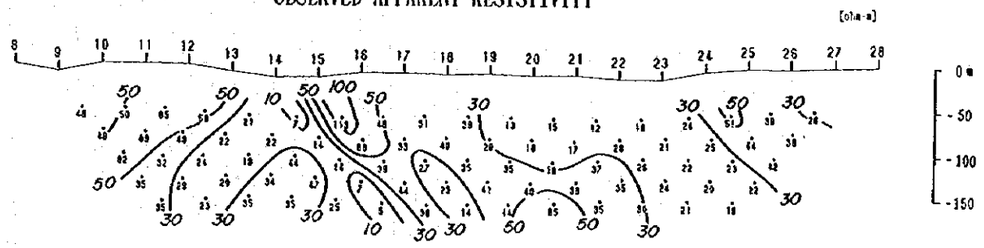

CHARGEABILITY

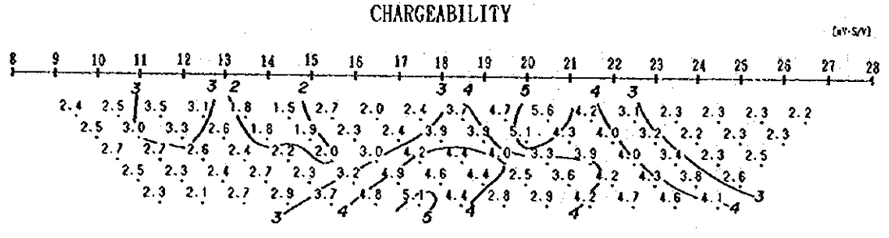

OBSERVED CHARGEABILITY

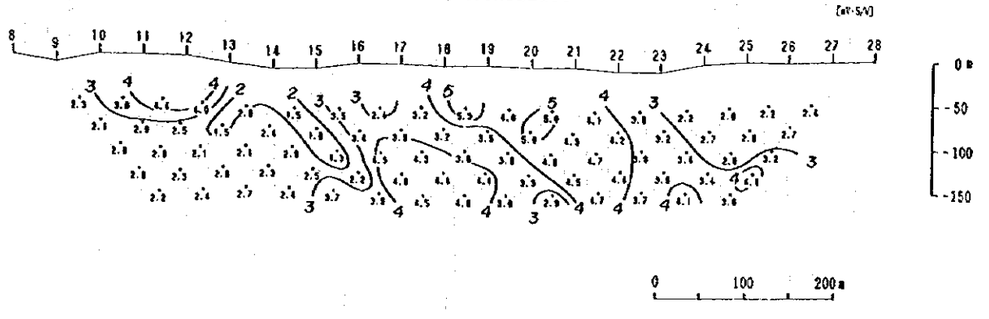

Fig. 2-33 Results of Two-Dimensional Model Simulation (Line K)

4-4-5 Discussion

Fig. 2-34 shows the geophysical interpretation map of the survey area. Anomalies of the chargeability (more than 4.0 mV·S/V) related to the mineralization were detected mainly at following three location.

(a) south-western part of lines C and D
(b) south-western part of line A ((a)and(b)are located in Sukasari)
(c) middle part of line J, K and L (located in Bihbul)

These anomalies occur from shallow into deep zones (about 150 m below the surface) in distinct expanse, and were detected in the low resistivity background ranged from 5 to 30 ohm-m corresponding to the tuff of the Upper member of the Jampang formation. Especially the anomalies (a) occur in the very low resistivity (<10 ohm-m) zone which coincides with the gravity trough structure. The anomalies (c) occur at the margin of relative high resistivity (>30 ohm-m) area where the basement depth is considered to be shallower. From the results of the drilling and gravity survey, the basement depth is considered to be deeper than -200 msl (more than 250 -300 m bellow the surface) in Sukasari and shallower than -150 msl (less than 250 m below the surface) in Bihbul.

Groups of shallower and smaller scale anomalies extend from the anomalies (c) in the E-W direction arranging like right handed echelon. These are :

- in the vicinity of Nos. 11 and 16 on line I
- in the vicinity of No. 8 on line H

Other small anomalies occur in the vicinity of No. 5 on line E and No. 36 on line A.

These anomalies have no distinct relation to resistivity patterns and are not so different in resistivity from the low background, supposing that they are related to the mineralization with clay alteration. Silicification and sericite-chlorite alteration were confirmed at drill hole MIT-7 whose target is the shallow anomaly at No. 16 on line I. This type of alteration is expect to occur in anomalies. As the high chargeability at the vicinity of No. 8 on line H coincides with high resistivity, it may related to the mineralization with silicification. Large scale silicification, however, is difficult to consider from the resistivity structure of this area.

The three major anomalous area are interpreted as follows, supposing that the zone with more than 30 mV·S/V of chargeability is as the mineralization and the one with 6 -15 mV·S/V is as the weak mineralization from the results of the model simulation

Anomalies (a) : Corresponding to the high chargeability, mineralized zones of several-tens-meter-scale are expected in the deep zones below No. 10 and No. 16 of line D. The Anomaly below No. 16 continues to the deep zone of the adjacent line C with larger-scale and to line E. It leads that this mineralized zone probably extends about 400m in the NW-SE direction and the center of mineralization is expected to be near line C. The anomaly

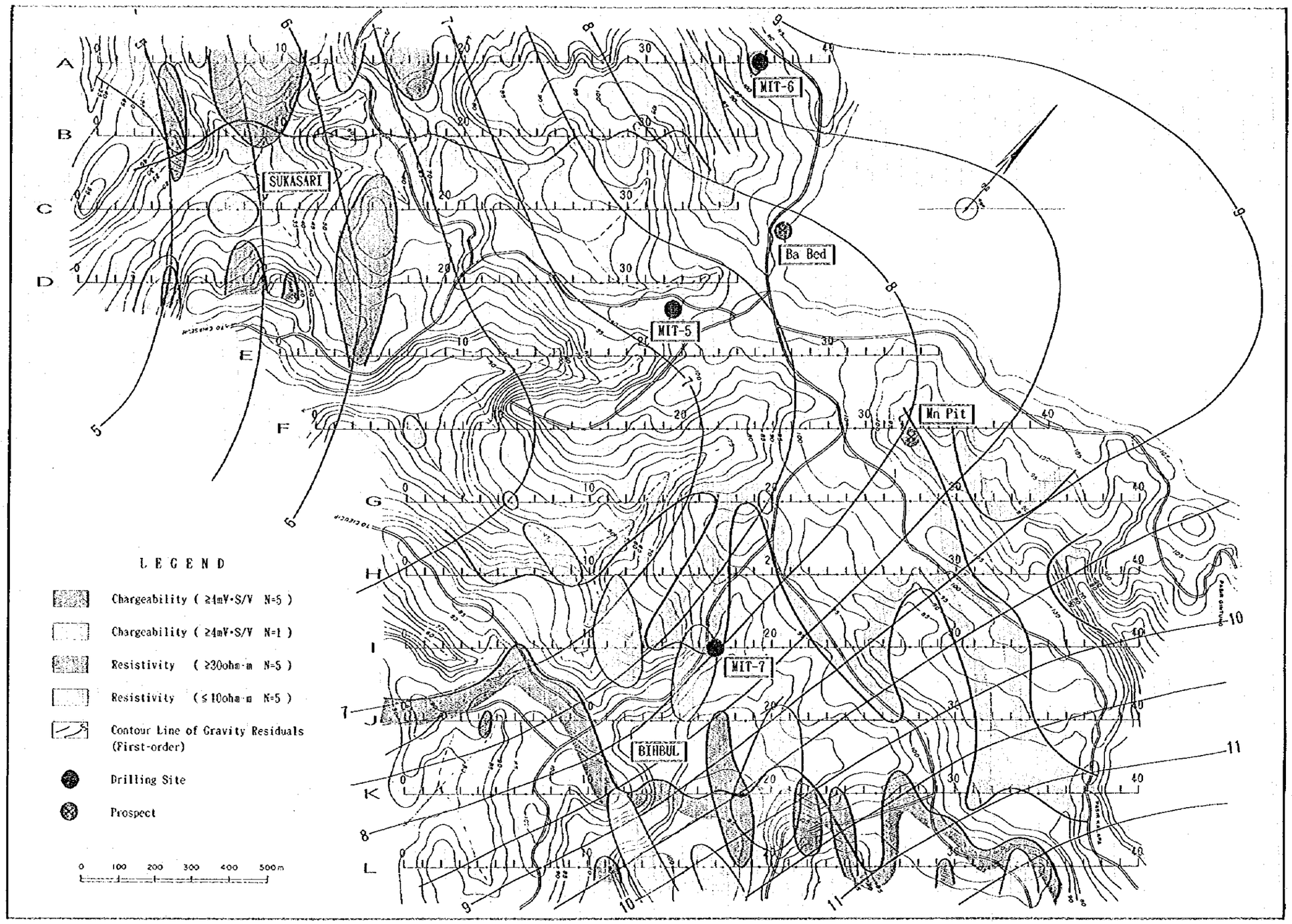

Fig. 2-34 Geophysical Interpretation Map (Cibuniasih Area)

below No. 10 is the one of the strongest on this survey, although the extension of the east side is not clear because of lack of survey lines. These two anomalies are most interesting for the further exploration, incorporating with locating in the local gravity trough structure. Another weak mineralized layer is supposed to exist in the shallow zone below No. 5.

Anomalies (b) : A mineralized zones with several-tens-meter-scale is supposed to exist in the deep zone below No. 11 of line A. This seems to extend in the SE direction to line B. Other inclined mineralized layers are supposed to exist in the middle depth zone below No. 5 and No. 18 of line A. Extension of these three anomalies to west and anomalies at the southern-end of line A are not understood because of lack of survey lines.

Anomalies (c) : A relatively weak mineralized layer is supposed to exist in the shallow zone below No. 20 of line K. This mineralization seems to extend in the NW direction to line J. As anomalies at lines I, H and G were detected only in the shallower zones, this stratified relatively weak mineralization in the shallow depth may be a common feature in Bihbul.

Another relatively weak mineralized layer is supposed to be in the middle depth zone below No. 26 of line K. A mineralized zone with several-tens-meter-scale may exists in the deep zone below No. 18 of line K. Because of existence of stratified weak mineralization mentioned above, however, accurate interpretation of the deeper part is difficult.

The predominantly low resistivity ranged from 5 to 30 ohm-m in the survey area was supported by the results of the laboratory test to tuff of the Upper member of Jampang Formation. One of the reason for its low resistivity is considered to be originated from widespread montmorillonitized tuff .

Chapter 5 Drilling

5-1 Outline of Drilling

In the second phase, a diamond drilling program comprising seven holes totaling 1,650 m was planned in the Cisasah-Cidadap-Cibuniasih area: four holes totaling 900 m in the western part, and three holes totaling 750 m in the eastern part of the area.

The program consisted of two categories of drilling. The first group was aimed at investigating the geologic structure of basement rocks (Lower Member of Jampang Formation) and ore horizon (green tuff sequences). Two holes -- MIT-1 and 2 -- were provided for this category. The second group was directed toward the significant geological/geochemical and geophysical anomalous zones. Significant mineralized/altered zones near the Cisasah gypsum deposit, which were defined by geological and geochemical survey, were targeted by two holes -- MIT-3 and 4. Other significant mineralized/altered zones south of the Cibuniasih barite bed, which were delineated by geological, geochemical and IP geophysical surveys, were targeted by the remaining three holes -- MIT-5 to 7.

The drilling program was composed of seven vertical holes of 200 to 250 m deep each. Target depths were set at 100 to 200 m from the surface. All holes (except MIT-5) were drilled until the basement rocks were confirmed in the hole. Seven holes of 1,704.10 m in total length have been drilled in this phase. Details of each hole are summarized in the table below. The location map of drill holes is shown in Fig. 2-35.

Hole No.	Area	Location	Elevation	Azimuth	Inclination	Length
MIT-1	Western area	Singkir	125 m	0	-90	200.50 m
MIT-2	ditto	Panyairan	170	0	-90	200.50
MIT-3	ditto	Cipari	175	0	-90	250.50
MIT-4	ditto	Panyosogan	215	0	-90	311.10
MIT-5	Eastern area	Sukasari	85	0	-90	250.50
MIT-6	ditto	Sukasari	100	0	-90	250.50
MIT-7	ditto	Bihbul	95	0	-90	240.50
Total	7 holes					1,704.10 m

A series of drill logs of 1:200 scale was prepared, and the whole drill cores were photographed in color. Seventeen samples for ore assay were obtained. Eight elements (Au, Ag, Cu, Pb, Zn, Fe, Mn and Ba) were analyzed for ore assay. One hundred forty-two rock chip samples were examined for geochemical analysis (Au, Ag, Cu, Pb, Zn, As, Sb, Fe,

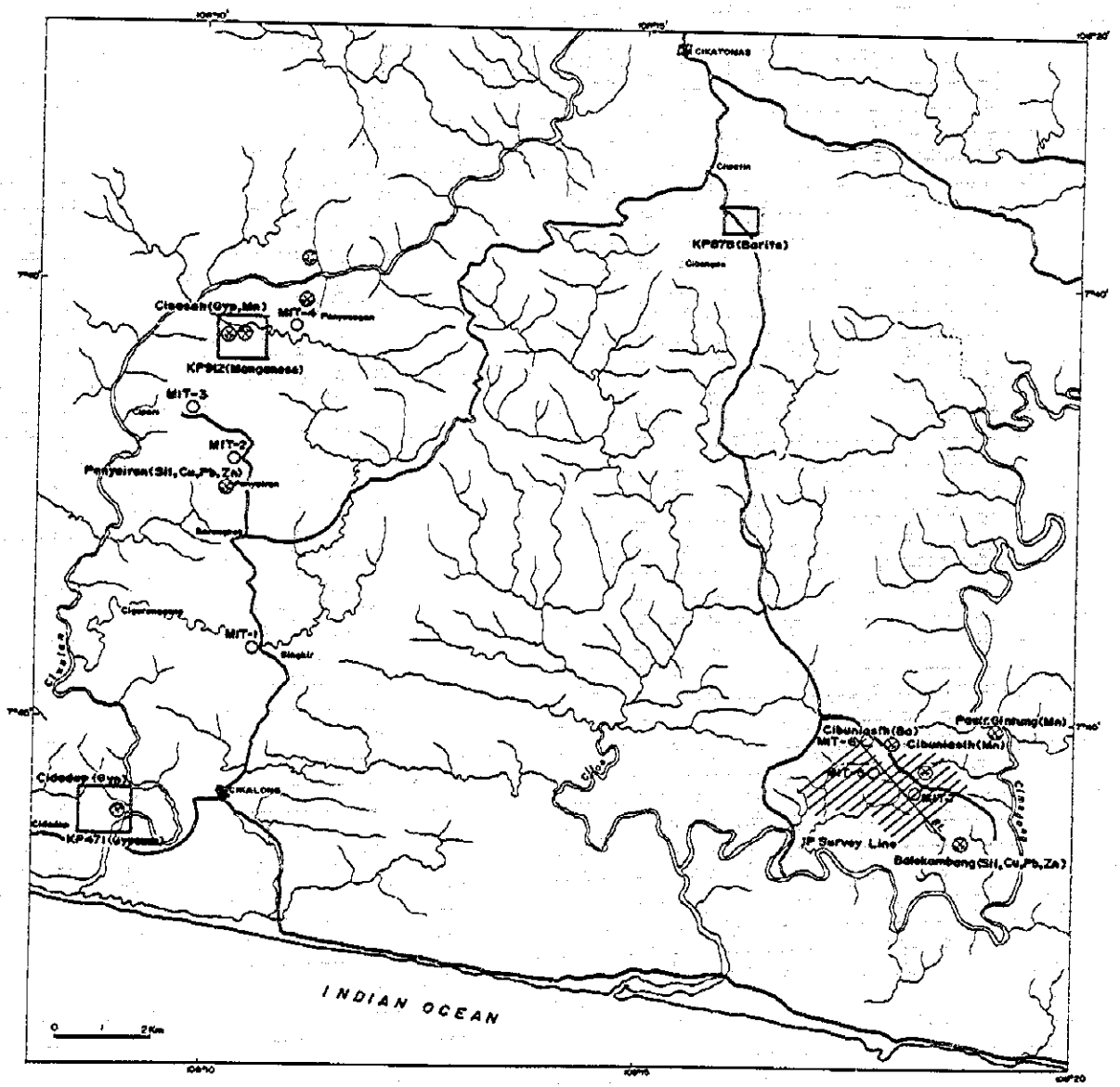

Fig. 2-35 Location Map of Drill Holes in the Cisasah-Cidadap-Cibuniasih Area

Mn, Ba, CaO, MgO, K_2O and Na_2O). Fifteen polished sections for ore microscopy and twenty-two thin sections for petrography were produced from the cores. Fifty-three altered rock and clay samples were examined for X-ray powder diffraction analysis.

5-2 Method and Equipment

Method

For surface soil and gravel layer (up to 6 m), drilling was done by HW metal casing shoe with inserting of HW casing pipes. Weathered bedrock and the upper part of bedrock zone were drilled by the conventional drilling method using NW diamond casing shoe. The weathered bedrock continued down to 8 m deep. NW casing pipes were inserted in this zone. For the upper part of bedrock zone, BW casing pipes were inserted down to approximately 100 m. From 100 m to 200 or 250 m (the end of hole), drilling was made with BQ oversized diamond bit (62.0 mm in outer diameter and 36.5 mm in inner diameter) and BQ-WL core tube. Bentonite mud, lubricant chemical (Mud Oil), Libonite and CMC were usually mixed in the circulating drilling water. When the water was lost in the hole where fractures were developed, Tel-Stop and Seaclay (asbestos) were injected to recover the trouble. Borehole cementation was applied where water loss and the collapse of wall happened at the same time.

Equipment

A set of Longyear L-38 drilling machine and Tone MG-15H drilling pump was brought into operation in this exploration. Specifications of drilling machine and equipment are shown in Table 2-9. Diamond bits and expendable items used during the drilling are listed in Tables 2-10 and 2-11 respectively.

Working System

Drilling operation was carried out by three shifts per day (8 hours per shift), while the appurtenant works, such as rig construction, mobilization and demobilization, were done by one shift per day. A shift crew consisted of one drilling engineer and five workers normally. Additional forty workers (round figures) were involved in case of the appurtenant work. A base camp for drilling operation was built in Cikatomas, a small town located north of the survey area. Commuting between the drilling site and base camp was made by cars. It took approximately 60 minutes in one way.

Table 2-9 Specifications of Drilling Machine and Equipments

Drilling Machine : Model L-38	1 set
Capacity	725 m (BQ-WL nominal)
Dimensions (L, W, H)	2,150 - 1,170 - 2,200 mm
Weight	2,200 kg
Hoisting Capacity	20,000 kg
Spindle Speed	100, 190, 320, 530 rpm
Engine : Model F3L912	38.0 ps/1,800 rpm
Drilling Pump : Model MG-15H	1 set
Pistone Diameter	68 mm
Stroke	75 mm
Capacity	120 l/min (discharge)
Dimensions (L, W, H)	2,900 - 720 - 1,120 mm
Weight	500 kg (excluding engine)
Engine : Model NFD-150	13.5 ps/2,400 rpm
Wireline Hoist : Model WLH-4	1 set
Drum Diameter	120 mm
Rope Capacity	1,200 m (6 mm diameter rope)
Dimensions (L, W, H)	1,130 - 450 - 1,000 mm
Weight	110 kg (excluding engine)
Engine : Model NFAD6	5.4 ps/2,600 rpm
Water Supply Pump: Model TA-900	1 set
Plunger Type	3 plunger lateral
Capacity	100 l/min (discharge)
Dimensions (L, W, H)	555 - 354 - 444 mm
Weight	30 kg (excluding engine)
Engine : Model LA90ASES	8.0 ps/1,800 rpm
Derrick : Model PD9.5	1 set
Height	9 m
Maximum Load Capacity	10,000 kg
Mud Mixer : Model MCF-200A	1 set
Capacity	200 l/800 rpm
Engine : Model NFAD6K	5.4 ps/2,600 rpm
Generator : Model YDG-3005S	3 sets
Capacity	2.7 KVA (100 V, 17 A)
Crane Carrier : Model YFC20	1 set
Load Capacity	1,700 kg
Crane Capacity	960 kg
Dimensions (L, W, H)	2,900 - 1,700 - 1800 mm
Weight	1,825 kg
Engine : Model NS75S	11.0 ps/2,500 rpm
Drilling Tools	
Drilling Rods	NQ-WL 3.0 m - 50 pcs
	BQ-WL 3.0 m - 140 pcs
Casing Pipes	HW CP 1.5 m - 4 pcs
	NW CP 3.0 m - 12 pcs
	BW CP 3.0 m - 60 pcs
Core Tubes	NQ-WL 3.0 m - 3 pcs
	NX-STH 1.5 m - 4 pcs
	BQ-WL 3.0 m - 5 pcs

Table 2-10 Drilling Meterage and Diamond Bit Consumption

Item	Size	Bit No.	Drilling Meterage/Each Bit							Total (m)
			MIT-1	MIT-2	MIT-3	MIT-4	MIT-5	MIT-6	MIT-7	
Diamond Bit	NQ	SINN-01	49.20							49.20
		SINN-02	49.40	13.10						62.50
		SINN-03		42.00						42.00
		SINN-04		25.10	24.70					49.80
		SINN-05			50.10					50.10
		SINN-06			20.20	34.70				54.90
		SINN-07				64.30				64.30
		SINN-08					46.40			46.40
		SINN-09					40.60	15.20		55.80
		SINN-10						51.00		51.00
		SINN-11						19.30	44.10	63.40
		SINN-12							20.00	20.00
		Total	98.60	80.20	95.00	99.00	87.00	85.50	64.10	609.40
			Average Drilling Length/Bit (m)					50.78		
	BQ	SINB-01	46.40							46.40
		SINB-02	52.00							52.00
		SINB-03		61.80						61.80
		SINB-04		54.90						54.90
		SINB-05			49.60					49.60
		SINB-06			82.00					82.00
		SINB-07			16.90	49.60				66.50
		SINB-08				54.00				54.00
		SINB-09				55.90				55.90
		SINB-10				49.60				49.60
		SINB-11					58.60			58.60
		SINB-12					56.90			56.90
		SINB-13					45.00	16.60		61.60
		SINB-14						69.00		69.00
		SINB-15						74.90		74.90
		SINB-16							48.70	48.70
		SINB-17							58.80	58.80
		SINB-18							42.80	42.80
		Total	98.40	116.70	148.50	209.10	160.50	160.50	150.30	1,044.00
			Average Drilling Length/Bit (m)					58.00		
Diamond Casing Shoe	NW	SINS-01	1.90	1.00	5.40					8.30
		SINS-02				1.50	2.00	3.50		7.00
		SINS-03							12.20	12.20
		SINS-04							12.90	12.90
		Total	1.90	1.00	5.40	1.50	2.00	3.50	25.10	40.40
			Average Drilling Length/Bit (m)					10.10		

Table 2-11 Consumption of Expendable Items

Expendable Items	Spec	Unit	Drill Hole No.							Total Amount
			MIT-1	MIT-2	MIT-3	MIT-4	MIT-5	MIT-6	MIT-7	
Diesel fuel		l	1,195	1,095	1,240	1,810	1,635	1,060	1,075	9,110
Hydraulic oil		l	5	60	15	60	65	60	60	325
Engine oil		l	15	30	20	30	35	30	30	190
Grease		l	40	40	35	45	40	40	40	280
Bentonite		kg	1,575	1,675	1,525	1,525	1,300	875	650	9,125
CMC		kg	75	55	111	92	92	84	39	548
Seaclay		kg	52	19	49	50	15	73	20	278
Libonite BX		kg	0	119	196	174	161	133	148	931
Tel-Stop		kg	27	21	52	32	30	38	25	225
Mud-Oil		l	32	58	88	75	94	95	66	508
Cement		kg	300	300	300	350	300	300	300	2,150
Diamond bit	NQ	pcs	2	2	2	1	2	2	1	12
Diamond bit	BQ	pcs	2	2	3	3	3	2	3	18
Diamond reamer	NQ	pcs	2	2	2	3	2	3	3	17
Diamond reamer	BQ	pcs	2	3	3	3	3	3	3	20
Metal casing shoe	HW	pcs	1	-	-	1	-	-	-	2
Diamond casing shoe	NW	pcs	1	-	-	1	-	-	2	4
Core barrel assembly	NQ	pcs	1	-	-	-	1	-	-	2
Core barrel assembly	BQ	pcs	1	-	-	-	1	-	-	2
Core lifter	NQ	pcs	1	-	-	-	1	-	-	2
Core lifter	BQ	pcs	1	-	-	-	1	-	-	2
Core lifter case	NQ	pcs	1	-	-	-	1	-	-	2
Core lifter case	BQ	pcs	1	-	-	-	1	-	-	2
Inner tube	NQ	pcs	1	-	-	-	-	-	-	1
Inner tube	BQ	pcs	1	-	-	-	-	-	-	1
Inner tube stabilizer	NQ	pcs	1	-	1	-	1	-	1	4
Inner tube stabilizer	BQ	pcs	1	-	-	1	1	-	-	3
Thrust ball bearing	NQ	pcs	2	2	2	2	2	2	2	14
Thrust ball bearing	BQ	pcs	2	2	2	2	2	2	2	14
Cylinder liner	MG-15	pcs	1	1	1	1	1	1	1	7
Pistone rod	MG-15	pcs	1	-	-	1	-	-	1	3
Pistone rubber	MG-15	pcs	2	2	2	2	2	2	2	14
V-packing	MG-15	pcs	1	1	1	1	1	1	1	7
Wireline cable		m	400	-	-	-	-	-	-	400
Core case	NQ	pcs	16	12	15	15	13	13	13	97
Core case	BQ	pcs	10	12	15	22	17	17	15	108

Transportation

The drilling machine and equipment were shipped from Yokohama to Jakarta. After landed, they were transported to Cikatomas by a convoy of 10-ton trucks. Several light trucks (2 to 4 tons in capacity) were chartered for the transportation of drilling machine and equipment from the main road to the drilling sites. Some of the drilling sites were located far from truck roads. In such cases, which happened in the eastern part of the survey area where the drilling locations were determined on the result of the IP geophysical survey, rough roads were constructed from the existing road (almost footpath) to the sites. A little caterpillar carrier which could carry up to 1,500 kg was brought into loading-unloading and in-site transportation.

Supply for the camp was made once in a week. Fuel and foods were bought at Tasikmalaya, and were transported by chartered cars.

Drilling Water

Two methods were adopted for the water supply. In the western part of the survey area, drilling sites were located not far from rivers. Water for drilling was pumped up from the nearest river to the drilling site via hoseline. Whereas in the eastern part, there was no river which could provide enough amount of water to the drilling work. A tank truck, which carries water container of up to 3 tons and water pump, was chartered for the transportation of water from river to the drilling sites.

Withdrawal

After the completion of drilling program, the machine and equipment were withdrawn by trucks through the same route to Jakarta. Then they were shipped back to Yokohama. The drill holes were capped, and drilling sites were cleaned and reclaimed. The drilling cores, of which the half was taken for assay samples in some part, were kept in the storage house in the office of DMR, Bandung.